Resource

Cell Host & Microbe

Combined Human Genome-wide RNAi and Metabolite Analyses Identify IMPDH as a Host-Directed Target against *Chlamydia* Infection

Graphical Abstract

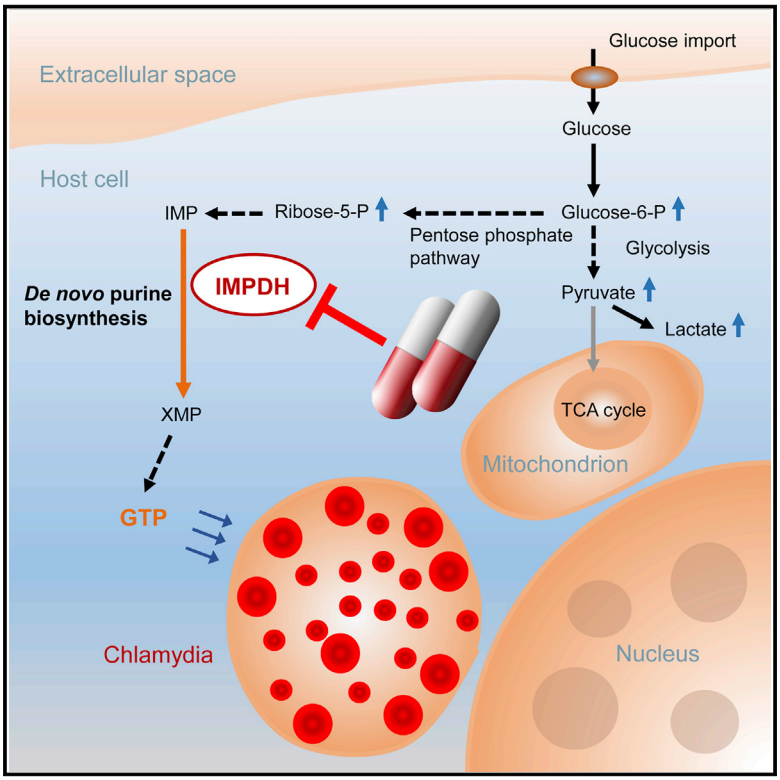

Authors

Marion Rother, Erik Gonzalez, Ana Rita Teixeira da Costa, ..., Bert Klebl, Andreas Klos, Thomas F. Meyer

Correspondence

meyer@mpiib-berlin.mpg.de

In Brief

Rother et al. integrated human genome-wide RNAi and metabolomics analyses to determine growth requirements and signaling routes essential for *Chlamydia trachomatis*, a highly prevalent human pathogen. They discover druggable host pathways and demonstrate that pharmacological targeting of the enzyme IMPDH efficiently inhibits *Chlamydia* growth *in vitro* and *in vivo*.

Highlights

- Human genome-wide loss-of-function RNAi screen for *Chlamydia* infection
- Superimposed metabolite analysis of the central carbon metabolism upon infection
- Map of host targets and pathways highlights Warburg metabolism during infection
- Targeting of host IMPDH efficiently blocks *Chlamydia* growth *in vitro* and *in vivo*

Rother et al., 2018, Cell Host & Microbe *23*, 661–671
May 9, 2018
https://doi.org/10.1016/j.chom.2018.04.002

CellPress

Cell Host & Microbe
Resource

Combined Human Genome-wide RNAi and Metabolite Analyses Identify IMPDH as a Host-Directed Target against *Chlamydia* Infection

Marion Rother,[1,2] Erik Gonzalez,[1] Ana Rita Teixeira da Costa,[1] Lea Wask,[3] Isabella Gravenstein,[1] Matteo Pardo,[1,4] Matthias Pietzke,[5,8] Rajendra Kumar Gurumurthy,[1] Jörg Angermann,[1] Robert Laudeley,[3] Silke Glage,[6] Michael Meyer,[1,2] Cindrilla Chumduri,[1] Stefan Kempa,[5] Klaus Dinkel,[7] Anke Unger,[7] Bert Klebl,[7] Andreas Klos,[3] and Thomas F. Meyer[1,9,*]
[1]Max Planck Institute for Infection Biology, Department of Molecular Biology, Charitéplatz 1, 10117 Berlin, Germany
[2]Center for Systems Biomedicine, Steinbeis Innovation, 14612 Falkensee, Germany
[3]Medical Microbiology and Hospital Epidemiology, Hannover Medical School, 30625 Hannover, Germany
[4]Institute for Applied Mathematics and Information Technologies, Italian National Research Council, 16149 Genova, Italy
[5]Integrative Metabolomics and Proteomics, Institute of Medical Systems Biology, Max Delbrück Center for Molecular Medicine, 13125 Berlin, Germany
[6]Institute for Laboratory Animal Science, Hannover Medical School, 30625 Hannover, Germany
[7]Lead Discovery Center GmbH, 44227 Dortmund, Germany
[8]Present address: Cancer Research U.K. Beatson Institute, Glasgow G61 1BD, UK
[9]Lead Contact
*Correspondence: meyer@mpiib-berlin.mpg.de
https://doi.org/10.1016/j.chom.2018.04.002

SUMMARY

***Chlamydia trachomatis* (*Ctr*) accounts for >130 million human infections annually. Since chronic *Ctr* infections are extremely difficult to treat, there is an urgent need for more effective therapeutics. As an obligate intracellular bacterium, *Ctr* strictly depends on the functional contribution of the host cell. Here, we combined a human genome-wide RNA interference screen with metabolic profiling to obtain detailed understanding of changes in the infected cell and identify druggable pathways essential for *Ctr* growth. We demonstrate that *Ctr* shifts the host metabolism toward aerobic glycolysis, consistent with increased biomass requirement. We identify key regulator complexes of glucose and nucleotide metabolism that govern *Ctr* infection processes. Pharmacological targeting of inosine-5′-monophosphate dehydrogenase (IMPDH), the rate-limiting enzyme in guanine nucleotide biosynthesis, efficiently inhibits *Ctr* growth both *in vitro* and *in vivo*. These results highlight the potency of genome-scale functional screening for the discovery of drug targets against bacterial infections.**

INTRODUCTION

Chlamydia trachomatis (*Ctr*) causes blinding trachoma (serovars A to C) and sexually transmitted infections that may result in pelvic inflammatory disease (PID; serovars D to L2). PID is considered the most serious and common complication of sexually transmitted diseases, where bacteria transmit upward into the uterus and beyond, and can cause tissue damage in the fallopian tubes, ovaries, and uterus. Tubal inflammation and scarring in particular is causally connected with ectopic pregnancy and infertility. Moreover, PID has been linked to the occurrence of ovarian cancer (Lin et al., 2011). Initially often asymptomatic, *Ctr* infections may turn into a chronic state that is refractory to antibiotic treatment. Reinfections are common, as are relapses due to the inability of antibiotics to completely eradicate bacteria, leading to severe chronic pathology. Such therapeutic failure is estimated to be ~10% (WHO, 2016).

Inside host cells, Chlamydiae are shielded within an inclusion vacuole, avoiding destruction by lysosomal fusion (Dautry-Varsat et al., 2004). Here they transform from extracellular, infectious elementary bodies (EBs) into replicative reticulate bodies (RBs), which multiply by binary fission, using the host cell's energy and nutrient resources. After multiple rounds of division, RBs transform back into EBs, which are released into the extracellular space to initiate new infection cycles (Hammerschlag, 2002).

Genome-wide RNAi Screen Identifies *Ctr* Host Factors

It remains largely unknown which cellular and metabolic processes are required to fuel *Chlamydia* growth. Comprehensive understanding of the functional contribution of host factors would provide insight into the molecular mechanisms of *Chlamydia* infection and enable the identification of targets for therapeutic intervention. We used a genome-wide RNAi screen targeting ~23,000 human genes to identify host factors with pivotal roles in *Chlamydia* infection (see Figure 1A for screen setup and Figure S1 for establishment of screening controls and data analysis). HeLa cells were chosen as a robust, screenable model of *Ctr* infection and transfected with small interfering RNAs (siRNAs), followed by infection with *Ctr* 3 days later. After 2 days, cells were lysed and infectious progeny titrated onto fresh cells. At 24 hr after reinfection, inclusions per nuclei were quantified by automated microscopy-based detection of immunolabeled *Ctr* inclusions and stained nuclei. In parallel, potential

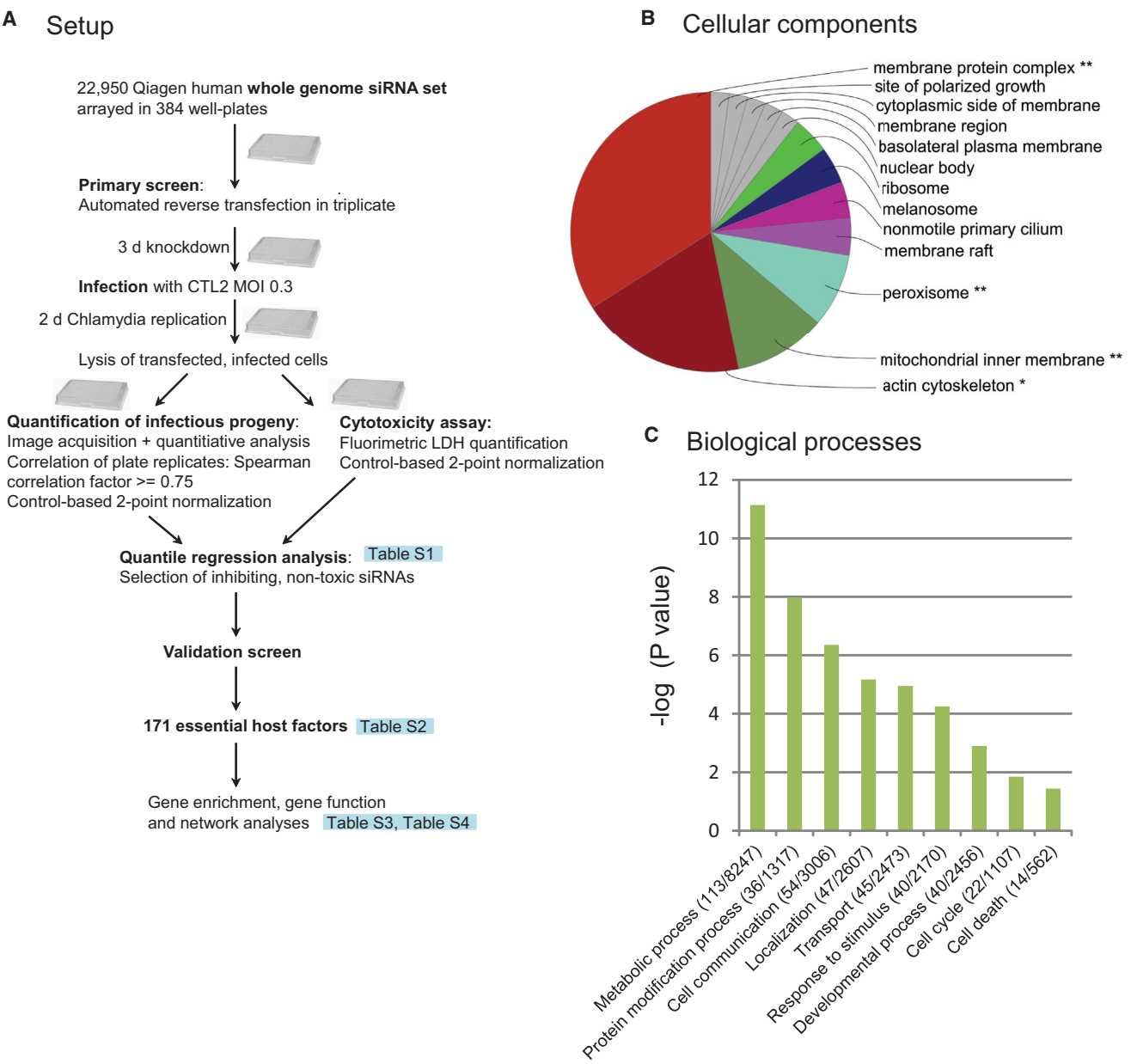

Figure 1. Human Genome-wide RNAi Screen Discovers Host Cell Factors Essential for *Chlamydia* Infection

(A) Assay setup and data analysis pipeline.

(B) Pie chart demonstrating overrepresented cellular components of validated hits determined with the ClueGO Cytoscape plug-in using the two-sided hypergeometric test for enrichment, Bonferroni correction, and for grouping % of genes per term versus cluster. **The term is highly significant with $p < 0.001$; *the term is significant with $0.001 < p < 0.05$.

(C) Classification of validated hits for selected enriched biological processes determined with PANTHER Overrepresentation Test (release 20150430, GO-Slim Biological Process with Bonferroni correction). Negative $\log_{10}$ ($p < 0.05$) are presented for each overrepresented term with numbers of identified factors per term and numbers of total genes associated with the term.

See also Figure S1 and Tables S1, S2, and S3.

siRNA cytotoxicity was assessed via lactate dehydrogenase (LDH) activity in the cell lysates. Quantile regression analysis of normalized infectivity and cytotoxicity data was used to identify strongly infection-inhibiting, non-cytotoxic siRNAs (see Table S1 for information on primary hits). In a subsequent validation screen, four independent siRNAs per hit candidate gene were applied in three experimental rounds, confirming 171 host cell factors as essential for *Ctr* infection (Table S2).

We classified the validated hits for enrichment of cellular components using the Cytoscape ClueGO application (Bindea et al., 2009; Cline et al., 2007), demonstrating membrane protein complex, actin cytoskeleton, mitochondrial inner membrane,

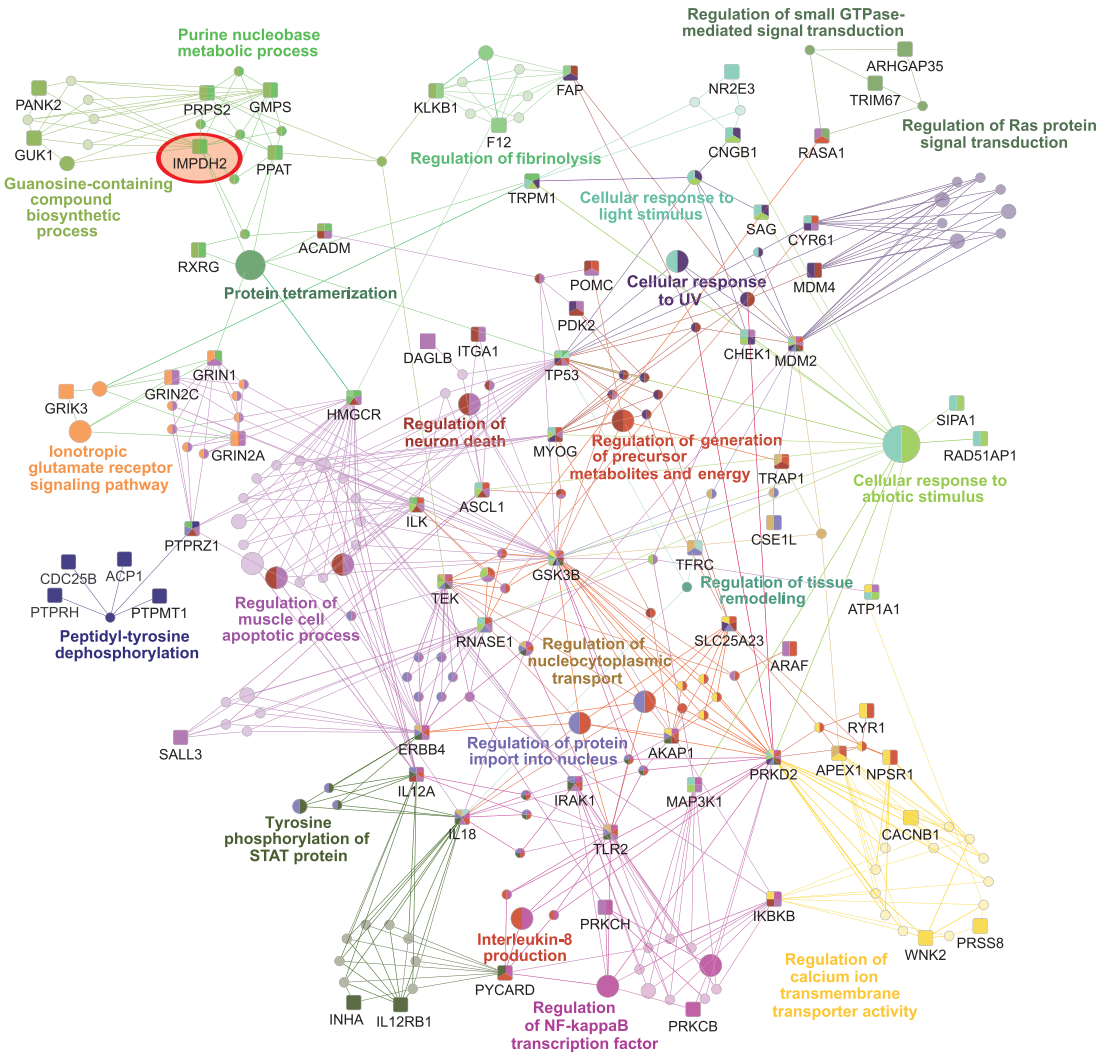

Guanosine-containing compound biosynthetic process
ACADM, GMPS, GUK1, IMPDH2, KLKB1, PANK2, PPAT, PRPS2, RXRG, TEK

Purine nucleobase metabolic process
GMPS, IMPDH2, PPAT

Protein tetramerization
ACADM, GMPS, GRIN1, HMGCR,IMPDH2,PPAT, PRPS2, RXRG, TP53,TRPM1

Ionotropic glutamate receptor signaling pathway
GRIK3, GRIN1, GRIN2A, GRIN2C, GSK3B, HMGCR, ILK, PTPRZ1, TRPM1

Regulation of fibrinolysis
F12, FAP, HMGCR, KLKB1

Peptidyl-tyrosine dephosphorylation
ACP1, CDC25B, PTPMT1, PTPRH, PTPRZ1

Regulation of generation of precursor metabolites and energy
AKAP1, APEX1, ARAF, ASCL1, CYR61, ERBB4, GSK3B, IL12A, IL18, ILK, IRAK1, MDM2, MYOG, NPSR1, POMC, PRKD2, PYCARD, RASA1, RNASE1, RYR1, SLC25A23, TEK, TLR2, TP53, TRAP1

Regulation of protein import into nucleus
AKAP1, CSE1L, ERBB4, GSK3B, IL12A, IL18, IRAK1, MDM2, PRKD2, PTPRZ1, RNASE1, SLC25A23, TEK, TFRC, TLR2

Tyrosine phosphorylation of STAT protein
AKAP1, ERBB4, GSK3B, IL12A, IL12RB1, IL18, INHA, IRAK1, MDM2, PRKD2, PYCARD, TEK, TLR2

Regulation of tissue remodeling
IL18, TFRC, TP53

Cellular response to UV
CHEK1,CNGB1, CYR61, FAP, GSK3B, MDM2, MDM4, MYOG, PDK2, PRKD2, SAG,SLC25A23,TP53, TRPM1

Cellular response to abiotic stimulus
ASCL1, ATP1A1, CHEK1, CNGB1, GSK3B, ILK, MAP3K1, MDM2, MYOG,PRKD2, RAD51AP1, RNASE1, SAG, SIPA1, TEK, TP53, TRPM1

Cellular response to light stimulus
ASCL1, ATP1A1, CHEK1, CNGB1, CYR61, GSK3B, MAP3K1, MDM2, MYOG, NR2E3, PRKD2, RAD5Ap1, RNASE1, SAG, SIPA1, TP53, TRPM1

Regulation of Ras protein signal transduction
ARHGAP35, RASA1, TRIM67

Regulation of NF-kappaB transcription factor activity
AKAP1, ERBB4, GSK3B, IKBKB, IL12A, IL18, IRAK1, MAP3K1, MDM2, PRKCB, PRKCH, PRKD2, PYCARD, TEK, TLR2

Regulation of neuron death
ACADM,AKAP1, ASCL1, FAP, GSK3B, HMGCR, IKBKB, IL12A,ILK, ITGA1, MDM2, MDM4, MYOG, PDK2, POMC, PRKD2, PTPRZ1, SLC25A23, TP53, TRAP1

Regulation of nucleocytoplasmic transport
APEX1, CSE1L, ERBB4, GSK3B, IL18, MDM2, TEK, TFRC, TLR2, TRAP1

Regulation of calcium ion transmembrane transporter activity
AKAP1, APEX1, ATP1A1, CACNB1, GSK3B, IKBKB, NPSR1, PRKD2, PRSS8, RYR1, SLC25A23, WNK2

Regulation of muscle cell apoptotic process
ACADM, RAF, ASCL1, ATP1A1, CHEK1, CYR61, DAGLB, ERBB4, GRIN1, GRIN2A, GRIN2C, GSK3B, HMGCR, IKBKB, IL12A, IL18, ILK, IRAK1, ITGA1, MAP3K1, MDM2, MYOG, PDK2, POMC, PRKCH, PRKD2, PTPRZ1, RASA1, RNASE1, SALL3, TEK, TLR2, TP53

(legend on next page)

and peroxisome as the most significantly overrepresented cellular components (Figure 1B and Table S3A). The biological processes governed by the hits were characterized using the PANTHER classification system (Thomas et al., 2003). Among all categories, the term metabolic process is most overrepresented, with 113 of the 171 validated hits, $p = 7.29 \times 10^{-12}$ (Figure 1C and Table S3B). Detailed analysis of enriched categories using the ClueGO (Bindea et al., 2009) Cytoscape (Cline et al., 2007) application revealed significantly grouped networks of gene ontology terms and pathways that are functionally interconnected (Figure 2), including networks with biosynthetic and modulatory roles in host metabolism, as well as signaling events, including apoptosis, nuclear factor-κB and glutamate receptor signaling, nucleocytoplasmic transporter functions, and calcium ion transporter activities (Table S4).

Ctr Modulates Host Energy and Nucleotide Metabolism

Several of our hits are enriched in the regulation of host cell precursor metabolites and energy, as well as in the guanosine-containing compound biosynthetic process (Figure 2). This is in congruence with the fact that *Ctr* substantially depends on energy supplied by the host (Eisenreich et al., 2013; Gehre et al., 2016; Iliffe-Lee and McClarty, 1999; Mehlitz et al., 2016; Omsland et al., 2014; Siegl et al., 2014). A major source of cellular energy and new cell mass is glucose, via oxidation to pyruvate in the glycolytic pathway, generating ATP and NADH, or through the formation of glycolytic intermediates that feed into biomass production (Lunt and Vander Heiden, 2011). However, little is known about which host cell functions involved in these metabolic processes are modulated upon infection.

Warburg Metabolism in Infected Cells

We therefore profiled metabolites of the central carbon metabolism upon *Ctr* infection. Cells were infected with serovar CTL2 at MOI 1 for 12, 24, 36, and 48 hr and metabolites analyzed using gas chromatography-mass spectrometry (GC-MS; Table S5). Subsequently, an interactive pathway map between cellular metabolism and essential host factors discovered by genome-scale RNAi functional screening was elaborated (Figure 3). In order to correct for continued cell growth during the time-course experiments, we calculated the ratio between infected and non-infected samples for each time point. Single time-course analyses for each detected metabolite are displayed in Figure S2. Notably, we observed strongly elevated levels of pyruvate, lactate, and glutamate upon *Ctr* infection. Increase in these metabolites resembles features of the Warburg metabolism, characterized by a higher rate of aerobic glycolysis, a process that involves the transformation of glucose to lactate even in the presence of sufficient amounts of oxygen. Aerobic glycolysis is upregulated in cells requiring increased biomass production, such as rapidly proliferating cells and cancer cells (Vander Heiden et al., 2009). Intriguingly, in our screen we identified pyruvate dehydrogenase kinase 2 (PDK2), a mitochondrial enzyme regulating aerobic glycolysis and the Warburg metabolism (Wu et al., 2013; Zhang et al., 2015), as an essential host factor for the formation of *Ctr* infectious progeny. Under normal, anaerobic glycolytic conditions, the end product of glycolysis, pyruvate, is mostly converted into acetylcoenzyme A (AcCoA), which enters the tricarboxylic cycle (TCA) cycle in the mitochondria in a process catalyzed by the pyruvate dehydrogenase complex (PDH). Phosphorylation by PDKs blocks this process, leading to accumulation of pyruvate. As a consequence, more pyruvate is converted into lactate by LDH, while at the same time more glycolytic intermediates can be shuttled into the pentose phosphate pathway (PPP) for ribonucleotide synthesis. This is irrespective of the observed increases in TCA cycle metabolites that might derive from different metabolic sources, such as glutamate, rather than from glycolysis. Thus, similar to what takes place in cancer cells, *Ctr* renders its host cell in a hypermetabolic state featuring aspects of the Warburg effect, thereby adjusting the host's metabolism to meet the high metabolic demands of rapid *Ctr* growth.

In contrast to what was believed for many years, the genomics era and the sequencing of the genome of *Chlamydiaceae* has shown that they are capable of fractional metabolic activity (Stephens et al., 1998), e.g., production of pyruvate from glucose-6-phosphate (G6P) via glycolysis, generating ATP. However, *Chlamydiaceae* lack hexokinase and therefore depend on the import of G6P from the host cytosol. Remarkably, we observed that G6P is highly upregulated upon infection and also identified the host glycolytic enzymes glucose-6-phosphate isomerase (GPI) and 6-phosphofructokinase (PFKM) as high-confidence hits in the primary screen, demonstrating that *Ctr* depends on active host glycolysis to raise levels of pyruvate and ATP.

Along similar lines, we also identified thiamine pyrophosphokinase isoform 1 (TPK1) as an essential host factor that generates thiamine pyrophosphate (TPP). TPP is a cofactor for transketolase (TKT) in the non-oxidative branch of the PPP (Liu et al., 2006; Patra and Hay, 2014), which generates ribose-5-phosphate (R5P) for *de novo* nucleotide metabolism. The PPP is required for synthesis of ribonucleotides and constitutes the major source of NADPH, which is needed for fatty acid synthesis and scavenging of reactive oxygen species (ROS). Thus, the PPP is crucial for meeting elevated anabolic demands, e.g., in rapidly proliferating cells, and to combat oxidative stress.

Ctr Upregulates Host Ribonucleotide Synthesis

The non-oxidative branch of the PPP recruits glycolytic intermediates, such as fructose-6-phosphate (F6P) and glyceraldehyde-3-phosphate (GA3P), derivatives of glucose-6-phosphate (G6P) and 3PGA, which are converted by transketolases into pentose phosphates to enter ribonucleotide biosynthesis. These steps

Figure 2. Pathway Network of Significantly Overrepresented GO Terms Based on Biological Processes of Validated Hits

The ClueGO Cytoscape application was used to decipher functionally grouped gene ontology and pathway annotation networks. GO terms are represented as nodes (circles), where the node size represents the statistical significance of the term enrichment based on the calculated p values. From all possible terms, the ones meeting the set criteria (GO level, # of genes and % of genes) are selected, and for those a p value was calculated using the Fisher's exact test. The terms are connected based on shared genes. Target genes associated with the nodes are presented as squares. A kappa score of 0.4 was used to define groups. Nodes with shared colors indicate connections to different groups. The name of each group is given by the group leading term (the most significant term in the group). See also Table S4.

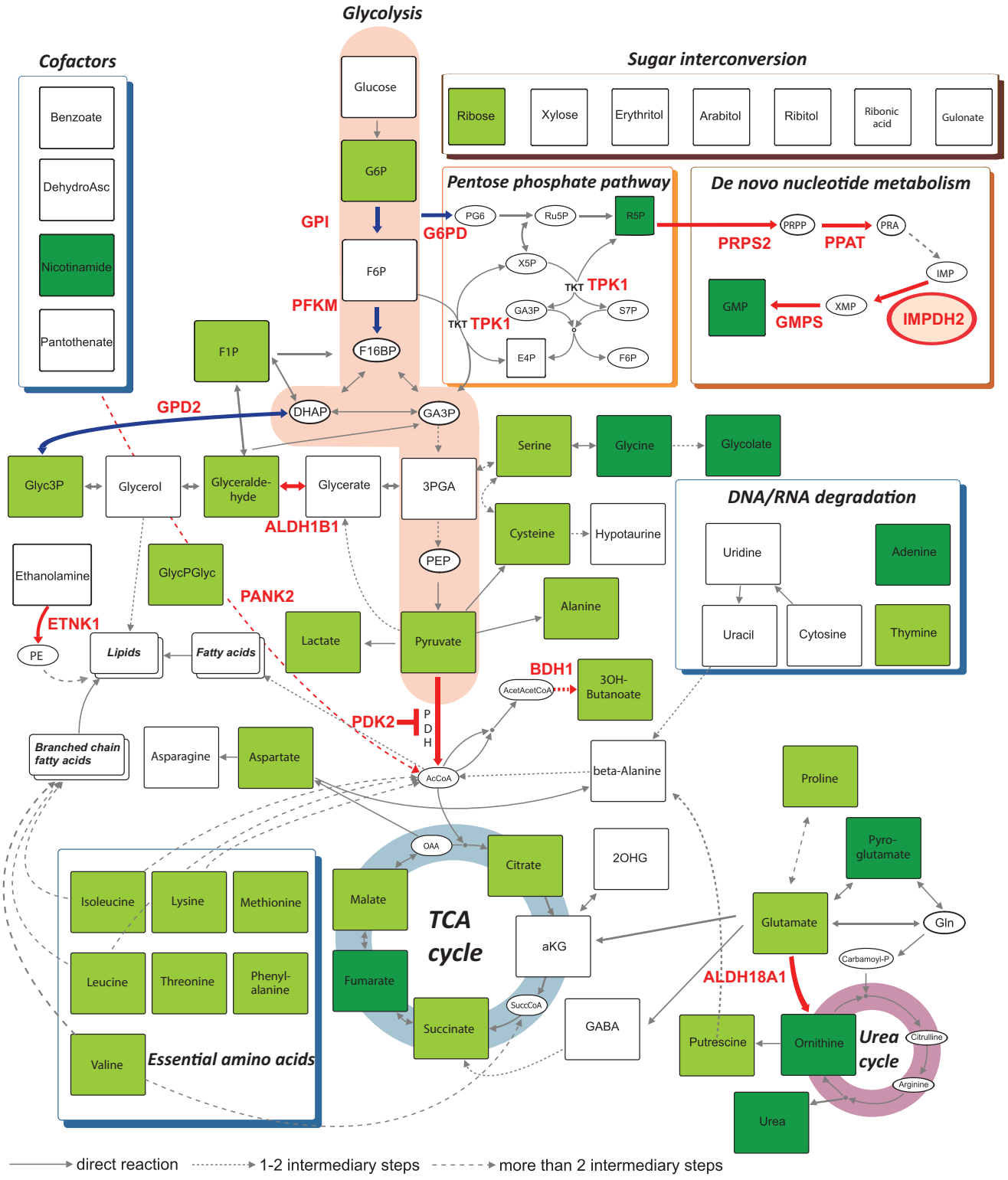

Figure 3. Systematic Representation of Modulated Metabolites and Related Host Cell Factors Essential for *Chlamydia* Infection in the Central Carbon Metabolism (48 hr p.i.)

HeLa cells were infected with CTL2 at MOI 1, or left uninfected, in three biological replicates. Data for a single time point are displayed in Table S5. A detailed description of the data normalization procedure is provided in the STAR Methods. Squares, detected metabolites 48 hr p.i.; light green squares, upregulated metabolites 48 hr p.i. with $p < 0.001$; dark green squares, upregulated metabolites with p values between <0.05 and >0.001, calculated by unpaired t test

(legend continued on next page)

are reversible, enabling the PPP to adapt to the metabolic demands of the cell and ensure a sufficient nucleotide supply. Buildup of glycolytic intermediates, as observed in our metabolic profiling for G6P, increases the carbon flux to alternative biosynthetic pathways, such as the PPP, for nucleotide biosynthesis and serine biosynthesis. The reliance of *Ctr* on the PPP is further confirmed by the identification of another high-confidence hit in the screen, G6P dehydrogenase (G6PD), which catalyzes the conversion of G6P into phosphogluconolactone (PG6), alongside a higher concentration of ribose-5-phosphate (R5P), the first metabolite to enter the nucleotide metabolism and elevated levels of guanosine monophosphate (GMP).

Nucleotides not only serve as building blocks for nucleic acids, but are also important for the synthesis of cofactors, such as FAD(H2), NAD(H), NADP(H), and coenzyme A (CoA). *Ctr* lacks enzymes of the *de novo* purine biosynthesis machinery and is therefore strictly dependent on the supply from the host. Biosynthesis of *de novo* purine nucleotides (ATP, GTP, dATP, dGTP) requires assimilation of ten carbon atoms from the extracellular environment. Half of these are derived from phosphoribosyl pyrophosphate (PRPP), the activated form of R5P, which is derived mainly from glucose and glycolytic intermediates (Lunt and Vander Heiden, 2011). The host factors identified in our screen are significantly enriched in *de novo* nucleotide metabolism, including four enzymes of the *de novo* purine metabolism, into which R5P feeds: phosphoribosyl pyrophosphate synthetase 2 (PRPS2), phosphoribosyl pyrophosphate amidotransferase (PPAT), inosine-5′-monophosphate dehydrogenase 2 (IMPDH2), and guanosine monophosphate synthetase (GMPS). The product of this metabolic pathway is guanosine monophosphate (GMP), which is further converted to guanosine diphosphate (GDP) and guanosine triphosphate (GTP).

Since cancer cells such as HeLa are known to have altered metabolic requirements, we further validated the requirement of these key metabolic host factors for *Ctr* replication in primary epithelial cells from the human ectocervix (Figures 4A–4D). To this end, we generated stable small hairpin RNA (shRNA)-mediated knockdown based on lentiviral transduction. For each of the four essential factors of the *de novo* purine metabolism, a significant reduction in infectivity was detected with at least two different shRNA sequences. There was a strict correlation between target knockdown efficiency and *Ctr* growth reduction, ruling out potential shRNA off-target effects (Figures 4A–4D). In addition, we explored the consequences of a complete loss of IMPDH2, the rate-limiting enzyme of the *de novo* guanosine nucleotide biosynthesis pathway, using CRISPR/Cas9 knockout technology. Single-cell HeLa clones with *IMPDH2* knockout were generated and complete loss of IMPDH2 protein confirmed by Western blot (Figures 4E and 4F). Notably, these clones were perfectly viable and revealed a substantial and robust block in *Ctr* infectivity, further substantiating the importance of this host factor. We conclude that in HeLa as well as primary cells, successful *Ctr* infection requires an intact *de novo* purine biosynthesis pathway and that PRPS2, PPAT, IMPDH2, and GMPS represent host factors essential for *Ctr* propagation.

Host Factor Targeting Is Effective *In Vitro*

To ensure that the identified host targets could provide a valid basis for the development of host-directed therapies, we performed extensive target prioritization using databases for chemical compounds and safety profiles in addition to the direct analysis in human primary cells. This led us to IMPDH2 as a promising target, which generates xanthine monophosphate (XMP) from inosine monophosphate (see also Figures 2 and 3, encircled in red). IMPDH2 can be specifically inhibited by the clinically approved and well-referenced compound mycophenolate mofetil (MMF), and thus constitutes an attractive candidate target for pharmaceutical intervention. MMF is the ester prodrug of mycophenolic acid (MPA) (Markham et al., 1999; Morath et al., 2006), a highly selective, non-competitive and reversible inhibitor of IMPDH (*in vitro* IC_{50} = 14 nm). To determine if MMF has antichlamydial effects, human HeLa cells were infected with CTL2 at MOI 0.3, and 4 hr later MMF was added at the indicated concentrations. In the presence of the inhibitor, *Ctr* replication and production of infectious progeny were completely abolished, even at nanomolar concentrations, in both human HeLa (Figures 5A, 5C, and 5D) and murine MLE 12 cells (data not shown). The drug elicited no cytotoxic effect (Figure 5B), demonstrating high efficacy in cell culture. Based on this titration, an IC_{50} of 20 nM was determined (95% confidence interval from 18 to 23 nM; *R* square = 0.99). The efficacy of MMF was confirmed in primary epithelial cells from the human ectocervix (Figure 5E) at concentrations of 1 and 10 μM, both of which significantly blocked infectivity. Infectivity could partly be rescued by simultaneous addition of 10 μM GMP, the specific purine product of the respective *de novo* metabolic pathway catalyzed by IMPDH2. No rescue of infectivity was observed, on the other hand, by addition of AMP (10 μM), a purine resulting from a different pathway branch, as a control. This confirms that

(see Table S5E); red arrows and red names, identified essential host factors for *Ctr* infection, validated; blue arrows, high-confidence host factors, identified in the genome-wide screen. See also Figure S2 and Table S5.

Abbreviations for metabolites: 2OHG, 2-hydroxyglutarate; 3OH-Butanoate, D-3-hydroxybutyrate; 3PGA, 3-phosphoglyceric acid; AcCoA, acetyl coenzyme A; AcetAcetCoA, acetoacetyl-CoA; aKg, alpha-ketoglutaric acid; Carbamoyl-P, carbamoyl-phosphate; DHAP, dihydroxyacetone phosphate; E4P, erythrose 4-phosphate; F16BP, fructose 1-6-bisphosphate; F6P, fructose 6-phosphate; G6P, glucose 6-phosphate; GA3P, glyceraldehyde 3-phosphate; GABA, γ-aminobutyric acid; Gln, glutamine; Glyc3P, glycerol 3-phosphate; GlycPGlyc, glycerophosphoglycerol; GMP, guanosine monophosphate; IMP, inosine monophosphate; OAA, oxaloacetic acid; PEP, phosphoenolpyruvate; PG6, phosphogluconolactone; PRA, 5′-phosphoribosylamine; PRPP, 5-phospho-D-ribose α-1-pyrophosphate; R5P, ribose 5-phosphate; Ru5P, ribulose 5-phosphate; S7P, D-sedo heptulose 7-P; SuccCoA, succinyl coenzyme A; X5P, xylulose 5-phosphate; XMP, xanthine monophosphate, PE, phosphatidylethanolamine; DehydroAsc, dehydroascorbic acid.

RNAi screen hits: *ALDH18A1*, aldehyde dehydrogenase 18 family member A1; *ALDH1B1*, aldehyde dehydrogenase 1 family member B1; *ETNK1*, ethanolamine kinase 1; *G6PD*, glucose-6-phosphate dehydrogenase; GMPS, guanosine monophosphate synthetase; *GPD2*, mitochondrial glycerol-3-phosphate dehydrogenase; *GPI*, glucose-6-phosphate isomerase; *IMPDH2*, inosine-5′-monophosphate dehydrogenase 2; *PDH*, pyruvate dehydrogenase; *PDK2*, pyruvate dehydrogenase kinase isoform 2; *PFKM*, 6-phosphofructokinase; *PPAT*, phosphoribosyl pyrophosphate amidotransferase; *PRPS2*, phosphoribosyl pyrophosphate synthetase 2; *TKT*, transketolase; *TPK1*, thiamine pyrophosphokinase 1; *BDH1*, 3-hydroxybutyrate dehydrogenase, type 1.

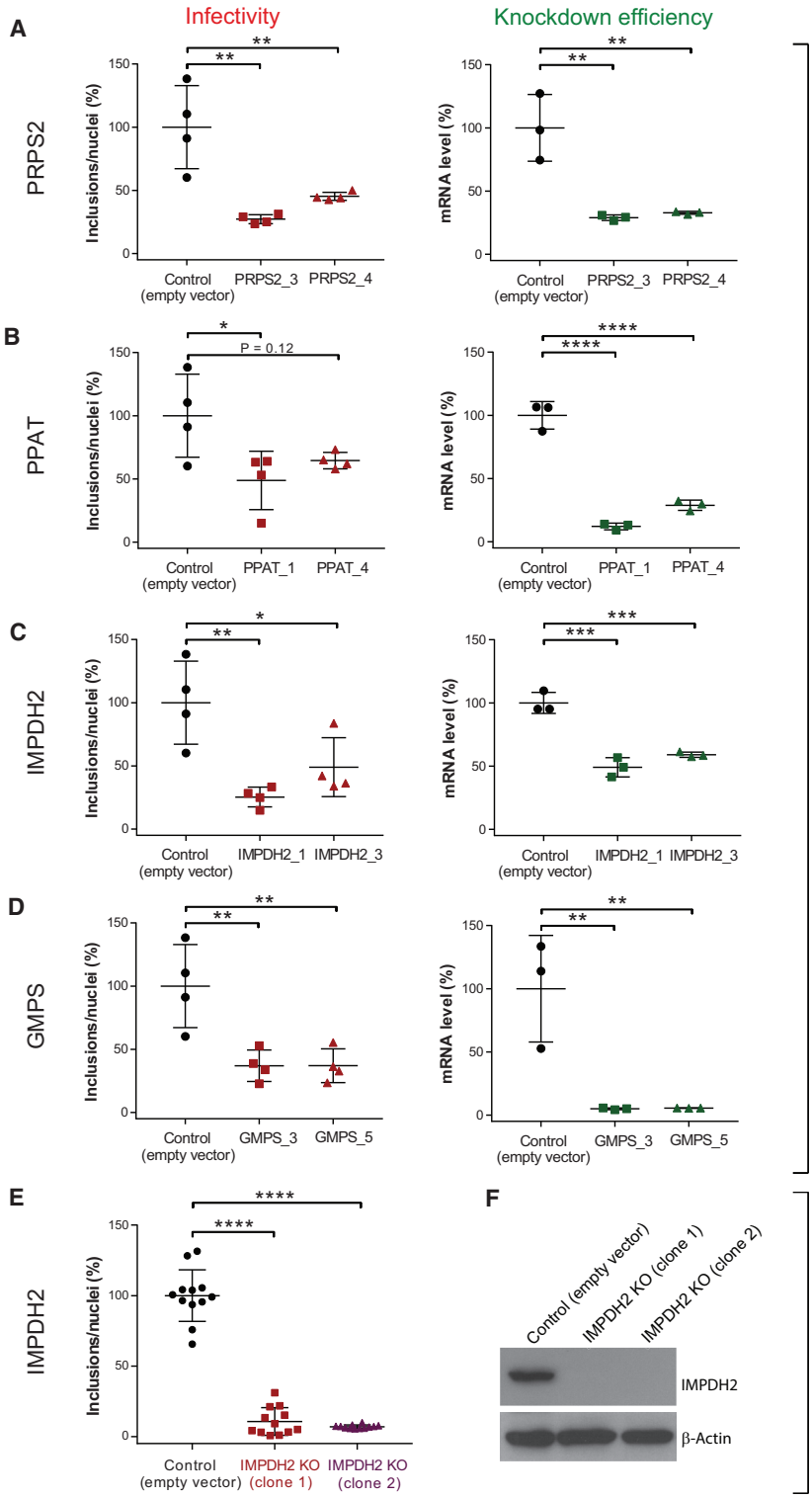

Figure 4. Validation of Key Screening Hits

(A–D) Primary ectocervical cells with a stable shRNA-mediated knockdown were generated for the four enriched key hits in the *de novo* nucleotide metabolism with two independent shRNA sequences per target gene. Cells were infected with CTL2 at M0I 0.3, and 48 hr p.i. infectious progeny assay was performed and knockdown efficiency determined. Results represent four technical replicates for infectivity determination and three replicates for evaluation of knockdown efficiency. For CRISPR/Cas9 knockouts, results represent three biologically independent experiments with four technical replicates each; target protein levels were analyzed by Western blotting. Infectivity and mRNA levels for shRNA knockdown of (A) *PRPS2* (phosphoribosyl pyrophosphate synthetase 2), (B) *PPAT* (phosphoribosyl pyrophosphate amidotransferase), (C) *IMPDH2* (inosine-5′-monophosphate dehydrogenase 2), (D) *GMPS* (guanosine monophosphate synthetase).

(E) Infectivity of *IMPDH2* knockouts compared with control (empty vector). Two single-cell HeLa CRISPR/Cas9 knockout clones were tested.

(F) Western blot of IMPDH2 and β-actin demonstrating IMPDH2 protein loss in the CRISPR/Cas9 knockout clones.

Data represent means ± SD. p values were calculated by one-way ANOVA followed by Bonferroni correction for multiple comparisons. *p < 0.05; **p < 0.01; ***p < 0.001; ****p < 0.0001.

the effect of MMF on *Ctr* infectivity is mediated via its effect on IMPDH2. Thus, while the purine salvage pathway might be adequate to ensure host cell survival, as demonstrated by the viability of our IMPDH2 knockout cells, the very high nucleotide demand required for intracellular bacterial replication cannot be met without *de novo* synthesis. These results in human primary cells are in accordance with the known drug mechanism of MMF.

Targeting of IMPDH Is Effective *In Vivo*

In order to identify a suitable dosing regimen for an *in vivo* efficacy study, we analyzed the pharmacokinetic (PK) profile of the active metabolite MPA after MMF dosing of 2 mg/kg intravenous (i.v.) and 40 mg/kg *per os* (PO) (Figure S3A). MPA shows low clearance (Cl = 0.17 L/hr/kg), a good half-life ($t_{1/2}$ = ~7 hr) and approximately 10% oral bioavailability. Based on the plasma protein binding, PK profile and the *in vitro* efficacy of MPA, a twice-daily dose of 200 mg/kg PO of MMF was predicted by pharmacokinetic/pharmacodynamic (PK/PD) modeling to ensure a continuous target inhibition of approximately 90%. To provide proof of concept for *in vivo* efficacy in the context of a whole organism, MMF or buffer was applied orally in a valid *Ctr* mouse lung infection model, which is suited for such screening (Dutow et al., 2016). Importantly, on day 4 post infection (p.i.), the load of infectious *Ctr* in the mouse lungs was significantly reduced (Figure 6A), showing that infection of primary cells in the more complex *in vivo* setting also depends on *de novo* purine synthesis. In congruence with

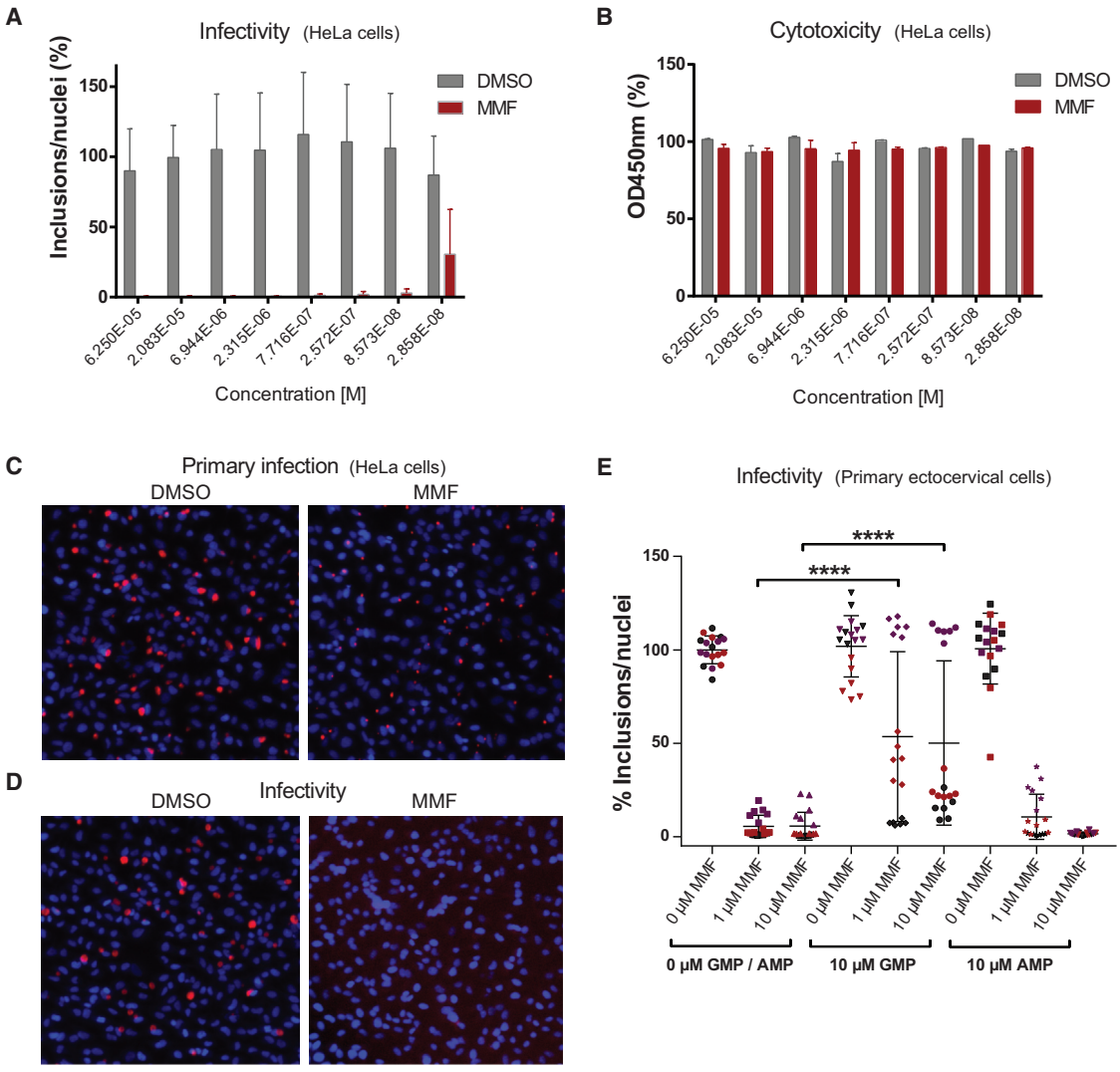

Figure 5. Targeting the Host *De Novo* Purine Metabolism via Blocking the Rate-Limiting Enzyme IMPDH MMF Efficiently Inhibits Bacterial Replication and Formation of Infectious Progeny in Cell Cultures

Efficacy of compound MMF in infected HeLa cells. Cells were seeded in 384-well plates and infected with CTL2 at MOI 0.3 for 4 hr. MMF was added in serial dilutions of 1:3 to achieve a dilution range between 62.5 µM and 28.6 nM. After 24 hr, one part of the samples was fixed for analysis of primary infection, the remaining part was lysed 48 hr after infection and infectious progeny was titrated onto fresh cells to determine infectivity. Data shown represent three values achieved in three independent biological experiments. For the compound MMF, an IC_{50} of 20 nM was calculated with 95% confidence interval from 18 to 23 nM and an *R* square of 0.99 (A). In addition, a WST-1 viability test was performed with the cell lysates (B). Data shown represent three values from three independent biological experiments. Immunofluorescence pictures of DMSO- and MMF-treated (250 nM) infected cells 24 hr after primary infection (C) and resulting infectivity (D). Nuclei, blue. *Chlamydia* inclusions, red. (E) Primary epithelial cells from the human ectocervix were infected with CTL2 at MOI 0.3. Four hours p.i., 1 and 10 µM MMF was added either in the presence or absence of 10 µM GMP or AMP. Infectious progeny assay was performed at 48 hr p.i. in order to determine infectivity. Three biologically independent experiments (indicated in different colors) with six technical replicates were performed. Data represent means ± SD. p values were calculated by one-way ANOVA followed by Bonferroni correction for multiple comparisons. ****$p < 0.0001$.

the reduced bacterial burden, body weight was significantly higher in MMF-treated animals (Figure S3E). Infection with *Ctr* serovar D produced similar results (data not shown). Lung pathology was determined in parallel, demonstrating normal morphology in uninfected, MMF-treated mouse lungs, while infected, buffer-treated mouse lungs showed severe infiltration of inflammatory cells into the stroma and alveoli, severe edema of the alveolar parenchyma, and activation of alveolar macrophages, as well as severe hyperplasia of Clara cells, the stem cells of the bronchiolar epithelium (Figure 6C). By contrast, in infected, MMF-treated mouse lungs, infiltration of inflammatory cells was strongly reduced, and bronchioles displayed only moderate Clara cell hyperplasia, resulting in a significantly reduced histological inflammatory score (Figure 6B; $p < 0.01$). In congruence with the lower number of bacteria and improved lung morphology, the levels of the key cytokines tumor necrosis factor alpha (TNF-α) and interferon gamma (INF-γ) were also significantly reduced (Figures S3B and S3C) and the

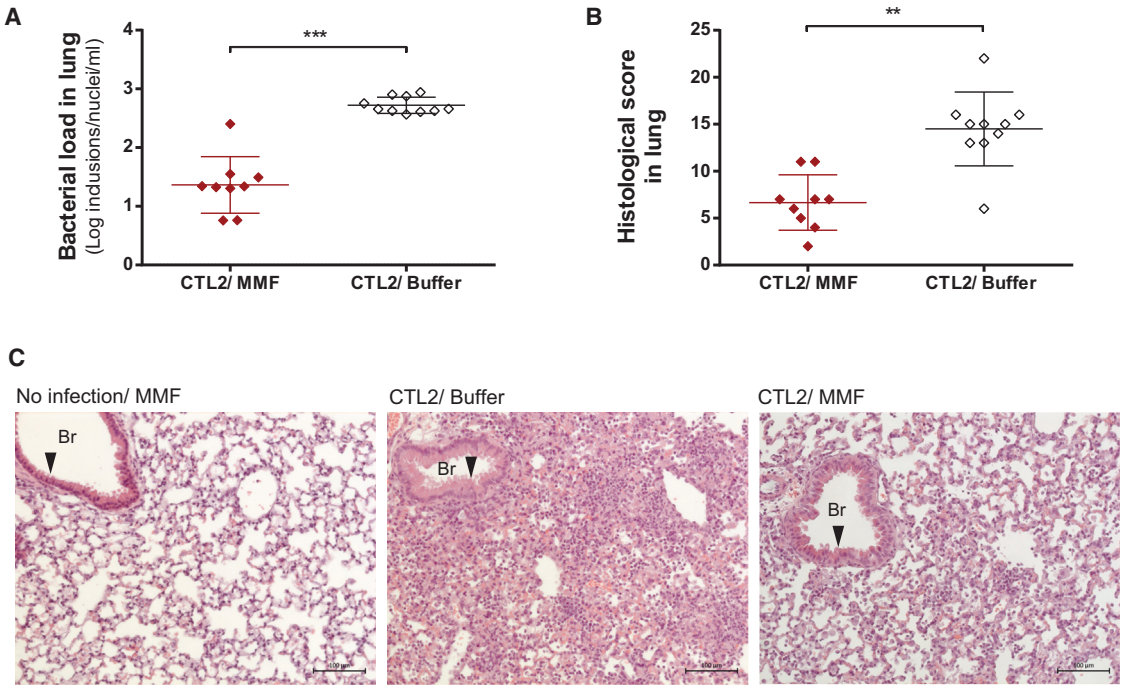

Figure 6. *In Vivo* Proof of Concept of Drug Action against *Ctr* Infection in the Context of a Whole Organism

Bacterial load (A) and histological score (B) after treatment of mice with MMF or buffer. Ten- to 12-week-old male C57BL/6J mice were intranasally infected with a CTL2 IFU of 8×10^5. MMF was applied orally twice daily using 200 mg per kg body weight starting 6 hr p.i. Infected control mice received only buffer. All mice were sacrificed on day 4 p.i. and homogenates from right lung lobes were assessed for bacterial load, left lung lobes were fixed, sectioned, and stained for histologic analysis. Mean and SD of n = 10 (buffer) or n = 9 (MMF) mice in each group are depicted, $^{**}p < 0.01$; $^{***}p < 0.001$. (C) Representative light microscopic images of H&E-stained lung sections from uninfected and MMF-treated, infected and buffer-treated, and infected and MMF-treated mice. Scale bars represent 100 μm. Br, bronchiole. MMF was also effective in mice infected with *Ctr* serovar D (data not shown). See also Figure S3.

concentration of the granulocyte marker enzyme myeloperoxidase (MPO) was diminished ($p < 0.001$), indicating reduced inflammation (Figure S3D).

It is likely that the decreased inflammatory parameters result not only indirectly from the reduced *Ctr* burden but also directly from the anti-inflammatory effect of MMF, e.g., via the reduction of rapidly proliferating B and T lymphocytes (Beduschi et al., 2013). However, the immunomodulatory effect of MMF, a well-tolerated drug used in long-term regimens for transplant and arthritis patients (Goldblum, 1993), does not necessarily diminish its potential value as an anti-infective against *Ctr*. In fact, it is uncertain if and to what extent adaptive immune cells, which are affected by MMF, rather than innate branches of the immune system contribute to the control of *Ctr* (Sturdevant and Caldwell, 2014). Reduced amplification of lymphocytes has also been shown to be favorable in a mouse model of sepsis where MMF supports both bacterial clearance and survival when combined with antibiotic treatment (Assfalg et al., 2010). Similarly, corticosteroids have proven useful in the treatment of both acute and chronic bacterial infections in conjunction with antibiotics (Brouwer et al., 2015; Prasad et al., 2016). Thus, our results provide a proof of concept for the validity of the host-directed approach against *Ctr* infections. Future optimization of the current MMF formulation for application in infections is likely to enable further increases in *in vivo* efficacy, e.g., via an enhancement of the local concentration at the site of infection.

DISCUSSION

The global exploration of host cell determinants and pathways exploited by *Ctr* provides comprehensive insight to further our mechanistic understanding of infections. A previous shRNA screen conducted with a guinea pig *Chlamydia* species in *Drosophila* cells revealed *Chlamydia caviae*-specific host factors that were demonstrated not to be important in *Ctr* infection (Derre et al., 2007). Besides, an insertional mutagenesis study performed in haploid mammalian cells revealed three factors involved in the attachment of *Ctr* to its host cell (Rosmarin et al., 2012). Thus, the data from the here presented genome-wide RNAi screen in mammalian cells establish a significantly advanced repository for future investigations on *Ctr* pathogenesis (Elwell et al., 2016). Moreover, we have elucidated a powerful strategy for the rapid identification of host targets suited for anti-infective treatments. Established drugs against identified targets constitute a rapid method to not only identify potential medications but to allow a quick assessment of their principle feasibility in animal models. While such screening-based drug repositioning strategies have been previously applied mainly for viruses (Karlas et al., 2016; Tripathi et al., 2015), here we demonstrate its validity for the experimental treatment of bacterial infections. Also, host-directed anti-infective strategies have previously been explored for other persistent bacteria, yet based on a rather more hypothesis-driven approach (Kaufmann et al., 2018; Mayer-Barber et al., 2014). Our genome-wide functional

assessment of *Ctr* host factor requirements provides ample opportunities for the discovery of additional drug target candidates. While host-cell-directed therapy offers a theoretical advantage over antibiotic treatment for preventing resistance development, it may also be suited for combinatorial treatment with antibiotics as well as in conjunction with vaccination. This will open up feasible approaches to assess the value of identified drugs in clinical settings.

STAR★METHODS

Detailed methods are provided in the online version of this paper and include the following:

- KEY RESOURCES TABLE
- CONTACT FOR REAGENTS AND RESOURCE SHARING
- EXPERIMENTAL MODEL AND SUBJECT DETAILS
  - Human Primary Ectocervical Cells
  - Cell Lines
  - Bacterial Strains
  - Animal Model
- METHOD DETAILS
  - Infections and Infectious Progeny Assay
  - High-throughput Screening of the Human Genome
  - Indirect Immunofluorescence Labelling
  - Automated Microscopy and Image Analysis
  - Determination of Cytotoxicity
  - Metabolite Profiling
  - Isolation of Human Primary Cells and Propagation
  - shRNA-Based Stable Knockdown in Human Primary Cells
  - CRISPR/Cas9 Knockout Cell Line Generation
  - Rescue Experiments with GMP and AMP
  - Western Immunoblotting
  - Determination of Compound Efficacy
  - Pharmacokinetics
  - PK/PD Modeling
  - *In Vivo* Studies
  - Lung Histology
- QUANTIFICATION AND STATISTICAL ANALYSIS
  - Screen Data Analysis and Hit Scoring
  - Validation of Host Cell Genes
  - Gene Enrichment and Network Analyses
  - Analysis of Metabolic Data
  - Analysis of *In Vivo* Experiments
- DATA AND SOFTWARE AVAILABILITY

SUPPLEMENTAL INFORMATION

Supplemental Information includes three figures and six tables and can be found with this article online at https://doi.org/10.1016/j.chom.2018.04.002.

ACKNOWLEDGMENTS

We thank Christiane Dimmler and Claudia Rheinheimer for expert technical assistance, Prof. Dr. Valentin-Weigand from the University of Veterinary Medicine Hannover for supervision and support of L.W. at MHH, and Rike Zietlow for editing the manuscript. E.G. was supported by a Deutscher Akademischer Austauschdienst (DAAD) PhD scholarship. M.R. was supported by BMWi grant no. KF3149632LW4 and by the BMBF through the Infect-ERA project CINOCA (FK 031A409A). A.R.T.d.C. was supported by a Max Planck PhD fellowship. L.W., R.L., and A.K. were supported by BMWi grant no. KF3309801LW4.

AUTHOR CONTRIBUTIONS

M.R. and E.G. performed RNAi screening. M.R. and M. Pardo conducted the data analyses. A.R.T.d.C., E.G., M. Pietzke, and S.K. performed metabolic profiling. J.A., R.K.G., I.G., A.R.T.d.C., and M.R. performed shRNA knockdown and CRISPR/Cas9 knockout experiments. C.C. and R.K.G. established primary cell cultures. M.R., K.D., M.M., and B.K. performed the compound selection and testing. A.K., L.W., R.L., and A.U. designed and performed the mouse experiments and pharmacokinetic studies. S.G. conducted the histological analysis. M.R. conceptualized and wrote the manuscript. M.R. and T.F.M. conceived the project. T.F.M. supervised the project and revised the manuscript.

DECLARATION OF INTERESTS

The authors declare no competing interests.

Received: February 22, 2017
Revised: January 24, 2018
Accepted: April 6, 2018
Published: April 26, 2018

REFERENCES

Assfalg, V., Huser, N., Reim, D., Kaiser-Moore, S., Rossmann-Bloeck, T., Weighardt, H., Novotny, A.R., Stangl, M.J., Holzmann, B., and Emmanuel, K.L. (2010). Combined immunosuppressive and antibiotic therapy improves bacterial clearance and survival of polymicrobial septic peritonitis. Shock *33*, 155–161.

Beduschi, M.G., Guimaraes, C.L., Buss, Z.S., and Dalmarco, E.M. (2013). Mycophenolate mofetil has potent anti-inflammatory actions in a mouse model of acute lung injury. Inflammation *36*, 729–737.

Bindea, G., Mlecnik, B., Hackl, H., Charoentong, P., Tosolini, M., Kirilovsky, A., Fridman, W.H., Pages, F., Trajanoski, Z., and Galon, J. (2009). ClueGO: a Cytoscape plug-in to decipher functionally grouped gene ontology and pathway annotation networks. Bioinformatics *25*, 1091–1093.

Brouwer, M.C., McIntyre, P., Prasad, K., and van de Beek, D. (2015). Corticosteroids for acute bacterial meningitis. Cochrane Database Syst. Rev., CD004405.

Cline, M.S., Smoot, M., Cerami, E., Kuchinsky, A., Landys, N., Workman, C., Christmas, R., Avila-Campilo, I., Creech, M., Gross, B., et al. (2007). Integration of biological networks and gene expression data using Cytoscape. Nat. Protoc. *2*, 2366–2382.

Dautry-Varsat, A., Balana, M.E., and Wyplosz, B. (2004). Chlamydia–host cell interactions: recent advances on bacterial entry and intracellular development. Traffic *5*, 561–570.

Derre, I., Pypaert, M., Dautry-Varsat, A., and Agaisse, H. (2007). RNAi screen in *Drosophila* cells reveals the involvement of the Tom complex in *Chlamydia* infection. PLoS Pathog. *3*, 1446–1458.

Dutow, P., Wask, L., Bothe, M., Fehlhaber, B., Laudeley, R., Rheinheimer, C., Yang, Z., Zhong, G., Glage, S., and Klos, A. (2016). An optimized, fast-to-perform mouse lung infection model with the human pathogen *Chlamydia trachomatis* for in vivo screening of antibiotics, vaccine candidates and modified host-pathogen interactions. Pathog. Dis. *74*, https://doi.org/10.1093/femspd/ftv120.

Eisenreich, W., Heesemann, J., Rudel, T., and Goebel, W. (2013). Metabolic host responses to infection by intracellular bacterial pathogens. Front. Cell Infect. Microbiol. *3*, 24.

Elwell, C., Mirrashidi, K., and Engel, J. (2016). *Chlamydia* cell biology and pathogenesis. Nat. Rev. Microbiol. *14*, 385–400.

Gehre, L., Gorgette, O., Perrinet, S., Prevost, M.C., Ducatez, M., Giebel, A.M., Nelson, D.E., Ball, S.G., and Subtil, A. (2016). Sequestration of host metabolism by an intracellular pathogen. Elife *5*, e12552.

Goldblum, R. (1993). Therapy of rheumatoid arthritis with mycophenolate mofetil. Clin. Exp. Rheumatol. *11* (*Suppl 8*), S117–S119.

Hammerschlag, M.R. (2002). The intracellular life of Chlamydiae. Semin. Pediatr. Infect. Dis. *13*, 239–248.

Heckl, D., Kowalczyk, M.S., Yudovich, D., Belizaire, R., Puram, R.V., McConkey, M.E., Thielke, A., Aster, J.C., Regev, A., and Ebert, B.L. (2014). Generation of mouse models of myeloid malignancy with combinatorial genetic lesions using CRISPR-Cas9 genome editing. Nat. Biotechnol. *32*, 941–946.

Iliffe-Lee, E.R., and McClarty, G. (1999). Glucose metabolism in *Chlamydia trachomatis*: the 'energy parasite' hypothesis revisited. Mol. Microbiol. *33*, 177–187.

Karlas, A., Berre, S., Couderc, T., Varjak, M., Braun, P., Meyer, M., Gangneux, N., Karo-Astover, L., Weege, F., Raftery, M., et al. (2016). A human genome-wide loss-of-function screen identifies effective chikungunya antiviral drugs. Nat. Commun. *7*, 11320.

Kaufmann, S.H.E., Dorhoi, A., Hotchkiss, R.S., and Bartenschlager, R. (2018). Host-directed therapies for bacterial and viral infections. Nat. Rev. Drug Discov. *17*, 35–56.

Koenker, R. (2005). Quantile Regression (Cambridge University Press).

Koenker, R., and Hallock, K. (2001). Quantile regression: an introduction. J. Econ. Perspect. *15*, 43–56.

Kuich, P.H., Hoffmann, N., and Kempa, S. (2014). Maui-VIA: a user-friendly software for visual identification, alignment, correction, and quantification of gas chromatography-mass spectrometry data. Front. Bioeng. Biotechnol. *2*, 84.

Lin, H.W., Tu, Y.Y., Lin, S.Y., Su, W.J., Lin, W.L., Lin, W.Z., Wu, S.C., and Lai, Y.L. (2011). Risk of ovarian cancer in women with pelvic inflammatory disease: a population-based study. Lancet Oncol. *12*, 900–904.

Liu, J.Y., Timm, D.E., and Hurley, T.D. (2006). Pyrithiamine as a substrate for thiamine pyrophosphokinase. J. Biol. Chem. *281*, 6601–6607.

Lunt, S.Y., and Vander Heiden, M.G. (2011). Aerobic glycolysis: meeting the metabolic requirements of cell proliferation. Annu. Rev. Cell Dev. Biol. *27*, 441–464.

Markham, G.D., Bock, C.L., and Schalk-Hihi, C. (1999). Acid-base catalysis in the chemical mechanism of inosine monophosphate dehydrogenase. Biochemistry *38*, 4433–4440.

Mayer-Barber, K.D., Andrade, B.B., Oland, S.D., Amaral, E.P., Barber, D.L., Gonzales, J., Derrick, S.C., Shi, R., Kumar, N.P., Wei, W., et al. (2014). Host-directed therapy of tuberculosis based on interleukin-1 and type I interferon crosstalk. Nature *511*, 99–103.

Mehlitz, A., Eylert, E., Huber, C., Lindner, B., Vollmuth, N., Karunakaran, K., Goebel, W., Eisenreich, W., and Rudel, T. (2016). Metabolic adaptation of *Chlamydia trachomatis* to mammalian host cells. Mol. Microbiol. *103*, 1004–1019.

Morath, C., Schwenger, V., Beimler, J., Mehrabi, A., Schmidt, J., Zeier, M., and Muranyi, W. (2006). Antifibrotic actions of mycophenolic acid. Clin. Transplant. *20* (*Suppl 17*), 25–29.

Naldini, L., Blomer, U., Gallay, P., Ory, D., Mulligan, R., Gage, F.H., Verma, I.M., and Trono, D. (1996). In vivo gene delivery and stable transduction of nondividing cells by a lentiviral vector. Science *272*, 263–267.

Omsland, A., Sixt, B.S., Horn, M., and Hackstadt, T. (2014). Chlamydial metabolism revisited: interspecies metabolic variability and developmental stage-specific physiologic activities. FEMS Microbiol. Rev. *38*, 779–801.

Patra, K.C., and Hay, N. (2014). The pentose phosphate pathway and cancer. Trends Biochem. Sci. *39*, 347–354.

Pietzke, M., Zasada, C., Mudrich, S., and Kempa, S. (2014). Decoding the dynamics of cellular metabolism and the action of 3-bromopyruvate and 2-deoxyglucose using pulsed stable isotope-resolved metabolomics. Cancer Metab. *2*, 9.

Prasad, K., Singh, M.B., and Ryan, H. (2016). Corticosteroids for managing tuberculous meningitis. Cochrane Database Syst. Rev. *4*, CD002244.

Rosmarin, D.M., Carette, J.E., Olive, A.J., Starnbach, M.N., Brummelkamp, T.R., and Ploegh, H.L. (2012). Attachment of *Chlamydia trachomatis* L2 to host cells requires sulfation. Proc. Natl. Acad. Sci. USA *109*, 10059–10064.

Siegl, C., Prusty, B.K., Karunakaran, K., Wischhusen, J., and Rudel, T. (2014). Tumor suppressor p53 alters host cell metabolism to limit *Chlamydia trachomatis* infection. Cell Rep. *9*, 918–929.

Stephens, R.S., Kalman, S., Lammel, C., Fan, J., Marathe, R., Aravind, L., Mitchell, W., Olinger, L., Tatusov, R.L., Zhao, Q., et al. (1998). Genome sequence of an obligate intracellular pathogen of humans: *Chlamydia trachomatis*. Science *282*, 754–759.

Stewart, S.A., Dykxhoorn, D.M., Palliser, D., Mizuno, H., Yu, E.Y., An, D.S., Sabatini, D.M., Chen, I.S., Hahn, W.C., Sharp, P.A., et al. (2003). Lentivirus-delivered stable gene silencing by RNAi in primary cells. RNA *9*, 493–501.

Sturdevant, G.L., and Caldwell, H.D. (2014). Innate immunity is sufficient for the clearance of *Chlamydia trachomatis* from the female mouse genital tract. Pathog. Dis. *72*, 70–73.

Thomas, P.D., Campbell, M.J., Kejariwal, A., Mi, H., Karlak, B., Daverman, R., Diemer, K., Muruganujan, A., and Narechania, A. (2003). PANTHER: a library of protein families and subfamilies indexed by function. Genome Res. *13*, 2129–2141.

Tripathi, S., Pohl, M.O., Zhou, Y., Rodriguez-Frandsen, A., Wang, G., Stein, D.A., Moulton, H.M., DeJesus, P., Che, J., Mulder, L.C., et al. (2015). Meta- and orthogonal integration of influenza "OMICs" data defines a role for UBR4 in virus budding. Cell Host Microbe *18*, 723–735.

Vander Heiden, M.G., Cantley, L.C., and Thompson, C.B. (2009). Understanding the Warburg effect: the metabolic requirements of cell proliferation. Science *324*, 1029–1033.

WHO. (2016). WHO Guidelines for the Treatment of *Chlamydia trachomatis* (WHO). https://www.ncbi.nlm.nih.gov/books/NBK379707/.

Wu, C.A., Chao, Y., Shiah, S.G., and Lin, W.W. (2013). Nutrient deprivation induces the Warburg effect through ROS/AMPK-dependent activation of pyruvate dehydrogenase kinase. Biochim. Biophys. Acta *1833*, 1147–1156.

Zhang, W., Zhang, S.L., Hu, X., and Tam, K.Y. (2015). Targeting tumor metabolism for cancer treatment: is pyruvate dehydrogenase kinases (PDKs) a viable anticancer target? Int. J. Biol. Sci. *11*, 1390–1400.

Zhang, Y., Huo, M., Zhou, J., and Xie, S. (2010). PKSolver: an add-in program for pharmacokinetic and pharmacodynamic data analysis in Microsoft Excel. Comput. Methods Programs Biomed. *99*, 306–314.

Zufferey, R., Nagy, D., Mandel, R.J., Naldini, L., and Trono, D. (1997). Multiply attenuated lentiviral vector achieves efficient gene delivery in vivo. Nat. Biotechnol. *15*, 871–875.

STAR★METHODS

KEY RESOURCES TABLE

REAGENT or RESOURCE	SOURCE	IDENTIFIER
Antibodies		
Cy3-conjugated goat anti-mouse	Jackson Immunoresearch	Cat# 115-165-146; Lot number: 80241
Mouse monoclonal species-specific KK-12 IgG2a Ctr (anti-MOMP)	D. Grayston, University of Washington, Seattle, WA, USA	N/A
Rabbit monoclonal IMPDH2	Abcam	Cat# ab131158; RRID: AB_11156264
Mouse monoclonal anti-β-actin	Sigma	Cat# A2228; RRID: AB_476697
HRP-linked ECL anti-rabbit	Amersham	Cat# NA934; RRID: AB_772211
HRP-linked anti-mouse	Amersham	Cat# NA931; RRID:AB_772212
Bacterial and Virus Strains		
Chlamydia trachomatis serovar L2	ATCC	VR-902B
Chlamydia trachomatis serovar D	ATCC	VR-885
Biological Samples		
Human primary ectocervical cells	Department of Gynecology, Charité University Hospital, Berlin, Germany	N/A
Chemicals, Peptides, and Recombinant Proteins		
GMP	Sigma	Cat# G8377
AMP	Sigma	Cat# A1752
Amphothericin B	HyClone	Cat# SV30078.01
Gentamycin	Calbiochem	Cat# 345815
Vancomycin	Serva	Cat# 38125
Hoechst 33342	Sigma	Cat# 23491-52-3
Nonidet P40 (NP40)	Sigma	Cat# 74385
Collagenase type II	Calbiochem	Cat# 234155
TrypLE	Gibco	Cat# 12604021
HEPES	Invitrogen	Cat# 15630-056
GlutaMax	Invitrogen	Cat# 35050-038
B-27	Invitrogen	Cat# 17504-044
N2	Invitrogen	Cat# 17502048
Hydrocortisone	Sigma	Cat# H0888
Human EGF	Invitrogen	Cat# PHG0311
Human Noggin	Peprotech	Cat# 120-10C
Human FGF-10	Peprotech	Cat# 100-26-25
N-acetyl-L-cysteine	Sigma	Cat# A9165
Nicotinamide	Sigma	Cat# N0636
TGF-β R kinase inhibitor IV	Calbiochem	Cat# 616454
ROCK inhibitor Y-27632	Hölzel Diagnostika	Cat# M1817
Forskolin	Sigma	Cat# F6886
Penicillin/streptomycin	Gibco	Cat# 15140-122
Collagen	Sigma	Cat# C3867
Opti-MEM medium	Gibco	Cat# 31985070
Fugene 6	Promega	Cat# E2691

(*Continued on next page*)

Continued

REAGENT or RESOURCE	SOURCE	IDENTIFIER
HiPerfect	Quiagen	Cat# 301709; Lot. No. 127147353 and Lot. No. 136232611
Puromycin	Gibco	Cat# 52400
Esp3I restriction enzyme	ThermoFisher	Cat# FD0454
RMPI 1640 medium	Gibco	Cat# 52400
DMEM	Gibco	Cat# 10938
Advanced DMEM/F12	Gibco	Cat# 12634
Fetal calf serum	Biochrom AG	Cat# S0155
Glutamine	Gibco	Cat# 25030081
Sodium pyruvate	Gibco	Cat# 11360070
MMF	Sigma	Cat# M5255
CellCept®	Roche	N/A
Hematoxylin	Merck	Cat# 1051740500
Eosin	Merck	Cat# 1159350025
Methoxyamine	Sigma	Cat# 226904
Pyridine	Roth	Cat# 9729.3
MSTFA	Macherey-Nagel	Cat# 701270.110
Cinnamic acid	Sigma	Cat# S573108
Critical Commercial Assays		
CytoTox-ONE assay	Promega	Cat# G7890
WST-1 assay	Roche	Cat# 11644807001
Mouse INF-γ ELISA	Biolegend	Cat# 430801
Mouse TNF-α ELISA	Biolegend	Cat# 430901
Mouse MPO ELISA	HyCult Biotechnology	Cat# HK210-02
Experimental Models: Cell Lines		
HeLa cells	ATCC	CCL-2; RRID: CVCL_0030
NIH3T3 fibroblasts	ATCC	CRL1658; RRID: CVCL_0123
HEK 293T cells	ATCC	CRL3216; RRID: CVCL_0063
HEp-2 cells	ATCC	CCL-23; RRID:CVCL_1906
BHK-21 cells	ATCC	CCL-10; RRID: CVCL_1915
Experimental Models: Organisms/Strains		
Mice: male C57BL/6J	Charles River Laboratories	C57BL/6J (RRID: IMSR_JAX:000664)
Oligonucleotides		
Human genome-wide siRNA library	Qiagen	Human Druggable genome V2.0 Human Supplement V1.0 Human predicted Genes siRNA Set V1.0
siRNA oligonucleotides	See Table S6	See Table S6
shRNA oligonucleotides	See Table S6	See Table S6
gRNA oligonucleotides	See Table S6	See Table S6
Recombinant DNA		
pLKO lentiviral vector	Stewart et al., 2003	Addgene Cat# 8453
psPax2	Trono Lab Packaging and Envelope Plasmids	Addgene Cat# 12260

(*Continued on next page*)

Continued

REAGENT or RESOURCE	SOURCE	IDENTIFIER
pMD.2G (VSVG)	Trono Lab Packaging and Envelope Plasmids	Addgene Cat# 12259
pL-CRISPR.EFS.GFP plasmid	Heckl et al., 2014	Addgene Cat# 57818
Software and Algorithms		
R quantreg package version 5.21	R consortium	https://cran.r-project.org/web/packages/quantreg/index.html
ScanR Analysis	Olympus Soft Imaging Solutions	N/A
Ingenuity Pathways Analysis	Qiagen Bioinformatics	N/A
Cytoscape v3.2.1	Cline et al., 2007	N/A
ClueGO v2.1.7.	Bindea et al., 2009	N/A
Maui-VIA	Kuich et al., 2014	N/A
ChromaTOF	LECO	N/A
CHOP CHOP tool	http://chopchop.cbu.uib.no	N/A
Genedata Screener	Genedata	N/A
PKSolver	Zhang et al., 2010	N/A
PS: Power and Sample Size Calculations	http://biostat.mc.vanderbilt.edu/wiki/Main/PowerSampleSize	N/A
GraphPad Prism	GraphPad Software	N/A

CONTACT FOR REAGENTS AND RESOURCE SHARING

Further information and requests for resources and reagents should be directed to and will be fulfilled by the Lead Contact, Thomas F. Meyer (meyer@mpiib-berlin.mpg.de).

EXPERIMENTAL MODEL AND SUBJECT DETAILS

Human Primary Ectocervical Cells

Anatomically normal human ectocervical tissue from a 56-year old patient was obtained from the Department of Gynecology, Charité University Hospital, Berlin, Germany and used within 3 h after removal. Scientific usage was approved by the ethics committee of the Charité University Hospital, Berlin (EA1/059/15). Informed patient consent was obtained. Cells were maintained in supplemented media as outlined below.

Cell Lines

HeLa cells (ATCC CCL2; RRID: CVCL_0030; authenticated via short tandem repeat (STR) profiling by the DSMZ, Braunschweig, Germany) were maintained in RPMI 1640 medium (Gibco) supplemented with 10% fetal calf serum (FCS, Biochrom AG). NIH3T3 and HEK 293T cells were maintained in DMEM (Gibco) supplemented with sodium pyruvate (Gibco) and glutamine (Gibco).

Bacterial Strains

Infections with mycoplasma-free (PCR) *Chlamydia* were conducted using *Ctr* serovars L2 (CTL2, ATCC VR-902B) and D (CTD, ATCC VR-885). For propagation and purification of *Ctr,* HEp-2 cells (ATCC CCL-23; RRID:CVCL_1906) were infected at MOI 1 in RPMI 1640 medium containing 5% FCS and 1 μg/ml cycloheximide and incubated at 35°C. After 2 d, infected cells were disrupted by vortexing with glass beads. Host cell debris was removed by centrifugation (5 min at 2,000 *g* and 4°C) and the supernatant was centrifuged at 48,000 *g* for 40 min at 4°C. The pellet was washed with SPG buffer (220 mM sucrose, 3.8 mM KH_2PO_4, 7 mM K_2HPO_4, 5 mM L-glutamic acid, pH 7.4), centrifuged and resuspended in SPG buffer using a syringe. Aliquots of 20 to 100 μl were frozen at -80°C. For mouse lung infection experiments, bacterial stocks were prepared in BHK-21 cells (ATCC CCL-10; RRID: CVCL_1915) as recently described (Dutow et al., 2016).

Animal Model

Animal experiments were approved by the Local District Government (LAVES; permit numbers: 33.19-42502-04-13/1223), and performed following the German regulations of the Society for Laboratory Animal Science (GV-SOLAS) for protection of animal life and the European Health Law of the Federation of Laboratory Animal Science Associations (FELASA). Ten to 12-week old male C57BL/6J mice (wildtype; RRID: IMSR_JAX:000664) were acquired from Charles River Laboratories and adapted to

specific-pathogen-free (SPF) conditions at the L2/S2 animal facilities at Hannover Medical School for a minimum of two weeks. Groups to be directly compared with each other, e.g. mice infected with one serovar of *Ctr* and treated either with buffer or drug, were run repetitively in parallel, with similar groups sizes of n = 2 to n = 7 animals in each experimental run. Animals were assigned to the different experimental groups by chance. Before and during infection experiments, 2 to 6 mice were kept in a type 2L cage. Corresponding groups were kept in the same cage to minimize differences due to housing conditions.

METHOD DETAILS

Infections and Infectious Progeny Assay

Infections were conducted using *Ctr* serovars L2 (CTL2, ATCC VR-902B) and D (CTD, ATCC VR-885) at the indicated MOIs. Unless otherwise stated, 72 h post transfection cells were infected for 2 h in RPMI growth medium containing 5% FCS at 35°C. Medium was then replaced with fresh growth medium and cells were cultured for the indicated times at 35°C.

Infectious progeny assays were conducted as follows. Cells seeded in 384-well plates were infected with CTL2 and CTLD as described above. Infected cells were lysed at 48 h p.i. by adding Nonidet P40 (NP40) at a final concentration of 0.06% per well. Lysates were diluted in infection medium and transferred to fresh HeLa cells at a final dilution of 1:40. After 2 h medium was exchanged to 5% FCS RPMI containing amphothericin B (2.5 μg/ml; HyClone), gentamycin (50 μg/ml; Calbiochem) and vancomycin (50 μg/ml; Serva). Plates were incubated for 24 h at 35 C and 5% CO_2 and processed for immunolabelling. CTD-containing lysates were centrifuged at 920 x g for 30 min onto the cell monolayers to improve reinfection efficiency. For immunolabelling, Cy3-conjugated goat anti-mouse antibodies (1:200 Jackson Immunoresearch) and mouse monoclonal species-specific KK-12 IgG2a *Ctr* antibodies (1:10,000) obtained from D. Grayston, University of Washington, Seattle, WA, USA were used. Hoechst 33342 was obtained from Sigma. Infection experiments were performed in three independent biological experiments, unless stated otherwise in the respective figure legend.

High-throughput Screening of the Human Genome

Small interfering RNAs (siRNAs, 200 nM) were arrayed in 384-well plates at 4 μl per well. To each well 8 μl of RPMI 1640 medium containing HiPerfect (0.16 to 0.24 μl per well, depending on the reagent lot) were added. Following shaking for 1 min and 15 min incubation at room temperature, 30 μl of cell suspension, containing 900 cells were added per well to give a final siRNA concentration of 19 nM. Cells were incubated at 37°C and 5% CO_2 for 72 h, infected with CTL2 at MOI 0.3 to 0.5 and further incubated at 35°C and 5% CO_2 until fixation of primary infection at 24 h post infection (p.i.) and lysis and reinfection along with cytotoxicity determination at 48 h p.i., respectively. Fixed cells were stained and immunolabelled for nuclei and *Chlamydia* MOMP antigen and analysed using automated microscopy and image analysis software from Olympus (ScanR). Automated liquid handling pipetting steps were performed using a Biomek FXp Laboratory Automation Workstation (Beckman Coulter). The human genome-wide siRNA library (Qiagen) consisting of Human Druggable genome V2.0 (6,992 genes covered with four siRNAs per gene), Human Supplement V1.0 (~10,000 genes covered with two siRNAs per gene) and Human predicted Genes siRNA Set V1.0 (~6,000 genes covered with two siRNAs per gene) was used for screening. In total ~22,950 target genes were screened three times independently. RNA interference oligonucleotide siAllstars (scrambled, neutral control for screen), siGMPS (inhibitory control, 5'-AACAGAGAACTTGAGTGTATT-3'), siPLK1 (toxic control, 5'-CCGGATCAAGAAGAATGAATA-3') and transfection reagent HiPerfect were purchased from Qiagen.

Indirect Immunofluorescence Labelling

Cells were fixed with ice-cold MetOH and stored at 4°C until immunofluorescence labelling. After 30 min blocking with PBS containing 0.2% BSA and 0.05% Tween 20, cells were incubated with the primary antibody against *Ctr* species-specific KK-12 IgG2a (1:10,000) for 1 h, washed twice with PBS and incubated for 1 h with Cy3-conjugated goat anti-mouse secondary antibody (1:200) and 10 μg/ml Hoechst. After washing twice with PBS, the labelled plates were stored at 4°C until image acquisition.

Automated Microscopy and Image Analysis

The numbers of *Chlamydia*-infected host cells were determined using automated microscopy (Olympus Soft Imaging Solutions): Images were taken with DAPI and Cy3 filter sets (AHF-Analysetechnik). ScanR Analysis Software (Olympus Soft Imaging Solutions) was used to automatically identify and quantify *Chlamydia* inclusions and cell nuclei.

Determination of Cytotoxicity

For determination of cytotoxicity upon siRNA knockdown in host cells the CytoTox-ONE assay (Promega) was performed to determine overall LDH activity in cell lysates. 7 μl of CytoTox-ONE substrate were mixed with 7 μl of cell lysate obtained in the infectious progeny assays and incubated for 20 min at room temperature. Fluorescence was then measured using an Envision plate reader with excitation wavelength of 560 nm and emission wavelength of 590 nm.

Host cell viability upon compound treatment was determined by measuring glycolytic production of NAD(P)H in viable cells with WST-1 assay (Roche). 48 h after addition of compounds 4 μl WST-1 reagent was added to cells in 40 μl culture medium. After incubation for 2 h at 37°C the OD was measured at 450 nm.

Metabolite Profiling

HeLa cells were seeded and infected with CTL2 at MOI 1 for the indicated time points (12, 24, 36 and 48 h). For cell harvesting, cells were quickly flushed with washing buffer (140 mM NaCl, 5 mM HEPES, 2.5 g/l glucose + 4 mM glutamine). Cells were then immediately quenched with 5 ml ice-cold 50% methanol containing 2 μg/ml cinnamic acid (Sigma) for internal control and scraped into the solvent. The lysate was stored at −20°C. For metabolite extraction, 1 ml chloroform was added and samples were shaken for 1 h at 4°C, followed by centrifugation for 10 min at 5000 rpm and drying overnight in a speedvac. Then samples were dissolved in 600 μl 20% methanol, followed by 1 h shaking at 4°C, centrifugation for 10 min at 5000 rpm and drying of samples overnight in a speedvac. Samples were derivatised by adding 40 μl of methoxyamine hydrochloride solution (Sigma, 40 mg/ml in pyridine, Roth) and shaking for 90 min at 30°C. N-methyl-N-trimethylsilyl-trifluoroacetamide (MSTFA; Machery-Nagel; 120 μl/sample) was added and samples were shaken at 37°C for 1 h followed by 10 min centrifugation at maximum speed. Gas chromatography-mass spectrometry (GC-MS) measurement and the analysis were carried out as previously described (Pietzke et al., 2014). The GC-MS chromatograms were processed with the ChromaTOF software (LECO). Mass spectra data were extracted using the software tool Maui-VIA (Kuich et al., 2014).

Isolation of Human Primary Cells and Propagation

Human ectocervical tissue was washed with PBS, minced with surgical scissors and incubated in 0.5 mg/ml collagenase type II (Calbiochem) for 2.5 h at 37°C followed by TrypLE (Gibco) digestion for 15 min at 37°C. Dissociated tissue was pelleted and resuspended in Advanced DMEM/F12 (Gibco) and single cells were isolated by passing through a cell strainer. Cells were pelleted by centrifugation, resuspended in human ectocervical primary cell medium consisting of Advanced DMEM/F12, 12 mM HEPES (Invitrogen) and 1% GlutaMax (Invitrogen), supplemented with 1% B27 (Invitrogen), 1% N2 (Invitrogen), 0.5 μg/ml hydrocortisone (Sigma), 10 ng/ml human EGF (Invitrogen), 100 ng/ml human noggin (Peprotech), 100 ng/ml human FGF-10 (Peprotech), 1.25 mM N-acetyl-L-cysteine (Sigma), 10 mM nicotinamide (Sigma), 2 μM TGF-β R kinase Inhibitor IV (Calbiochem), 10 μM ROCK inhibitor Y-27632 (Hölzel), 10 μM forskolin (Sigma) and 1% penicillin/streptomycin (Gibco) for cell expansion in 75cm^2 flasks coated with collagen (Sigma). At 70-80% confluence, cells were passaged using TrypLE and seeded onto lethally irradiated NIH3T3 fibroblasts (ATCC CRL1658; RRID: CVCL_0123) in ectocervical primary cell medium. For *Chlamydia* infection and lentivirus transduction experiments human primary ectocervical cells were subjected to differential trypsinization to separate fibroblasts from epithelial cells and epithelial cells were seeded on plastic dishes coated with collagen.

shRNA-Based Stable Knockdown in Human Primary Cells

All shRNAs used in this study were purchased from Sigma. Recombinant lentiviruses expressing shRNAs were produced according to standard protocols using a three-plasmid lentivirus packaging system (Naldini et al., 1996; Zufferey et al., 1997). shRNA-containing pLKO lentiviral vectors (a gift from Bob Weinberg; Addgene plasmid # 8453 (Stewart et al., 2003)) were dissolved in Opti-MEM medium (Gibco) together with Fugene 6 (Promega) transfection reagent and psPax2 packaging plasmids (a gift from Didier Trono; Addgene plasmid # 12260, Trono Lab Packaging and Envelope Plasmids, unpublished) and pMD.2G (VSVG) envelope plasmids (a gift from Didier Trono; Addgene plasmid # 12259, Trono Lab Packaging and Envelope Plasmids, unpublished) and incubated for 20-30 min at RT. After incubation, liposomes formed were added to the cells in growth medium. Next day, medium was replaced and left for an additional 24 h at 37°C in 5% CO_2. Two days post transfection, lentiviral particles present in the medium were harvested, filtered (0.45 μm) and used for transduction of human primary ectocervical cells. Cells were seeded in 10 cm dishes one day before lentiviral particles were ready for use. At 30-40% cell confluence, lentiviral particles were added onto cells together with 8 μl of polybrene (10 mg/ml; Sigma) followed by medium exchange after overnight incubation. After four days of lentivirus transduction, 0.5 μg/ml of puromycin (Gibco) was added to select positively transduced cells. The expanded pools of transduced cells were used for determination of *Chlamydia* infectivity and knockdown efficiency by real-time PCR.

CRISPR/Cas9 Knockout Cell Line Generation

Guide RNAs (gRNAs) targeting IMPDH2 were designed using the CHOP CHOP tool (http://chopchop.cbu.uib.no/) and cloned into pL-CRISPR.EFS.GFP plasmid (a gift from Benjamin Ebert; Addgene plasmid # 57818 (Heckl et al., 2014)) after digesting the vector with Esp3I restriction enzyme. HEK 293T cells (ATCC CRL3216; RRID: CVCL_0063) were transfected with gRNAs containing pL-CRISPR.EFS.GFP plasmids together with packaging vectors to produce lentiviruses for transduction of HeLa cells. Briefly, HEK 293T cells were grown to 60-70% confluency in 10 cm plates and transfected with lentiviral constructs containing gRNA and lentiviral packaging plasmids (psPax2 and VSVG). The lentiviral vectors were dissolved in Opti-MEM medium together with Fugene 6 transfection reagent and packaging plasmids psPax2 and pMD.2G (VSVG) and incubated for 20-30 min at RT. After incubation, liposomes formed were added to the cells in growth medium. Next day, medium was replaced and left for another 24 h at 37°C in 5% CO_2. Two days post-transfection lentiviral particles present in the medium were harvested, filtered (0.45μm) and used for HeLa cell transduction. HeLa cells were seeded in 10 cm plates one day before lentiviral particles were ready for use. At 30-40% confluence lentiviral particles were added onto cells together with 8 μl of polybrene (10 mg/ml), followed by medium exchange after overnight incubation. After seven days of lentivirus transduction, GFP-positive cells were FACS-sorted and seeded as single cells into 96-well plates. Single cell clones of transduced cells were expanded, determined to be mycoplasma-free and used for infectivity and Western blot experiments.

Rescue Experiments with GMP and AMP

Human primary ectocervical cells were infected with CTL2 at MOI 0.3. Four hours post-infection MMF (0.1 and 10 μM) was added either in the presence or absence of 10 μM GMP and AMP (Sigma). After 48 h infectious progeny assay was performed to determine infectivity.

Western Immunoblotting

Cells were lysed in SDS lysis buffer (100 mM Tris/HCL pH 6.8, 4% SDS, 20% glycerol, 0.02% bromophenol blue, 10% 2-mercaptoethanol) and boiled at 90°C for 10 min. Equal amounts of protein were separated using SDS-PAGE and immunoblotted using rabbit monoclonal IMPDH2 antibodies (ab131158, 1:1,000 from Abcam) and mouse monoclonal β-actin antibodies (AC-15, 1:4,000–16,000, Sigma). Secondary HRP-linked ECL anti-rabbit (NA934, 1:3,000) and HRP-linked anti-mouse (NA931, 1:3,000) antibodies were obtained from Amersham.

Determination of Compound Efficacy

Compounds were serially diluted at a 1:3 ratio in 5% FCS RPMI to achieve eight different concentrations ranging from 62.5 μM to 29 nM and added to CTL2- and CTD-infected cells 5 h post infection. Infectivity and cytotoxicity were assayed and analysed as described above. Dose response curve fitting was performed using the Genedata Screener software.

Pharmacokinetics

MMF (CellCept®, Roche) was administered at a single dose of 2 mg/kg intravenously in 10% DSMO/80% saline and 40 mg/kg PO in 100% saline to three male C57BL/6J mice each. Plasma samples were obtained at 5, 15, 30, 60, 120, 240, 480 and 1440 minutes after administration and analyzed for the active metabolite. MPA was extracted from plasma by protein precipitation. Extracts were analyzed by liquid chromatography tandem-mass spectrometry using a Prominence UFLC system (Shimadzu) coupled to a QTrap 5500 instrument (ABSciex). MPA was separated using a C18 column and an acetonitrile/water gradient containing 0.1% formic acid as solvent. Chromatographic conditions and mass spectrometer parameters were optimized prior to measurement. MPA plasma concentrations were calculated by means of a standard curve. Pharmacokinetic parameters were calculated using PKSolver (Zhang et al., 2010).

PK/PD Modeling

MPA plasma concentrations obtained from oral administration were best fitted to the two-compartment model. Percent activity for given concentrations was calculated using the Hill equation (Hill slope = 1) and an *in vitro* IC50. All calculations were performed using unbound MPA concentrations (mouse plasma protein binding 90%).

In Vivo Studies

To test the effectiveness of the drug *in vivo*, a mouse lung infection model with CTL2 for *in vivo* screening of antibiotics was used as recently described (Dutow et al., 2016). Ten to 12-week old male C57BL/6J mice were intranasally infected with 8 × 105 CTL2 chlamydial IFU per mouse. MMF at a dosage of 200 mg/kg body weight was administered orally twice a day starting at 6 h p.i. (see arrows in the graph). Infected control mice received buffer instead. Body weight was determined daily. Four days p.i. and 12 h after the final application of MMF all mice were sacrificed; infectious burden and other laboratory parameters were analyzed in homogenates from right lung lobes. Thawed, diluted tissue homogenates were centrifuged onto monolayers of HeLa T cells (received from R. Heilbronn, FU Berlin, Germany; subclone of HeLa229, ATCC CCL-2.1; RRID:CVCL_1276) growing in 96 well plates. After 24 h of culture at 37°C cells were fixed with ice-cold MetOH and the bacterial load (MOI) was determined by immunofluorescence, automated microscopy and quantitative image analysis as described above. Mouse INF-γ and TNF-α were quantified using ELISA Kits (Biolegend) according to the manufacturer's instructions. The granulocyte marker enzyme myeloperoxidase was determined using the mouse MPO ELISA (HyCult Biotechnology). When an experiment was conducted with CTD serovar, an IFU of 8 × 106 per mouse was applied.

Lung Histology

Histologic analysis was performed as described recently (Dutow et al., 2016). Briefly, left lung lobes were fixed in 4% formaldehyde, sectioned, stained with Hematoxylin and Eosin (Merck, Darmstadt, Germany) and analyzed by light microscopy (Zeiss Axioskop 40). For determination of pneumonia-typical pathology, the degree of inflammation was scored according to the following parameters: inflammatory cells, edema, hemorrhaging, peribronchiolar infiltrates, affected area, luminal exudates and overall disease pathology. The first three parameters were rated with a value between 0 and 2 points; the other parameters were rated with a value between 0 and 5 points. The score was determined by adding all points, resulting in a score of 0 (not affected) to 26 (highly affected) points. All preparations were evaluated and graded in a blinded manner by a veterinary expert.

QUANTIFICATION AND STATISTICAL ANALYSIS

Screen Data Analysis and Hit Scoring

Data analysis of the three genome-wide screening rounds was performed using the Genedata Screener Analyzer software. A two-point percent-of-control normalization was applied using neutral, inhibiting and cytotoxic controls present on each screening

plate. The neutral control as central reference was set to zero and the inhibiting and toxic scale references to -100, respectively. Quality of screening data was assessed by calculation of robust Z' factors (0.56 for infectivity data and 0.49 for cytotoxicity data), demonstrating valid control performance on assay plates throughout the screening procedures. Spearman's rank correlation coefficient was determined on the plate replicates to determine reproducibility of data using the R programme. Replicates with a correlation coefficient $\geq$ 0.75 underwent further analysis as described below; in case the correlation was below this cut off, replicates were experimentally repeated until the criterion was met.

In order to identify critical, infectivity-inhibiting, non-cytotoxic siRNA sequences for determination of a candidate gene list for validation, for which effects are less prone to influences in variation of cell numbers and the inclusion of less false positives, a quantile regression (QR) analysis (Koenker, 2005; Koenker and Hallock, 2001) was performed on the normalized genome-wide cytotoxicity (LDH activity) and infectivity (*Chlamydia* inclusions per nuclei) data. We used the R quantreg package version 5.21 (https://cran.r-project.org/web/packages/quantreg/index.html) with splines as approximating functions. The optimal spline degree of freedom (DF) was determined with 5-fold cross-validation for each quantile of interest. We tested DFs from 5 to 50 with intermitting steps of 5. For every quantile of interest the DF corresponding to the minimal median error was selected and the QR recalculated on all data.

Based on the distribution of neutral, inhibiting and toxic siRNA controls, the selection was carried out as follows: All target genes derived from quantile 0.7 (with optimized degrees of freedom of 20), for which a $\geq$ 4-fold infectivity-inhibiting effect was observed with at least two different siRNA sequences and for which normalized cytotoxicity values were $\geq$ -70 were selected for validation. A couple of host factors were additionally selected by network analyses, resulting in a candidate list consisting of 380 candidate genes selected from quantile regression analysis and 25 candidate genes selected by network analyses that did not reach the significance limits in the primary screen, but which represented borderline candidates.

Validation of Host Cell Genes

For validation of candidate genes with essential function in *Chlamydia* infection, four independent siRNA sequences have been tested, typically with two siRNAs showing the most prominent effect in the genome-wide screen and two additional independent sequences. The validation screen was carried out in three rounds, determining nuclei numbers and infection rates in primary infection (inclusions per nuclei in knockdown cells 24 h p.i.) and infectivity. Data analysis and normalization was performed as described for the genome-wide screening data. Target genes that upon knockdown led to a $\geq$ 4-fold inhibition of infectivity with at least two different siRNA sequences and $\geq$ 300 nuclei per well image present in primary infection were scored as validated.

Gene Enrichment and Network Analyses

Gene ontology and enrichment analyses were performed using PANTHER classification system (Thomas et al., 2003), network and enrichment analyses were implemented using Ingenuity Pathways Analysis software and Cytoscape v3.2.1 (Cline et al., 2007) with the ClueGO v2.1.7. (Bindea et al., 2009) application.

Analysis of Metabolic Data

Mass spectra data were extracted using the software tool Maui-VIA (Kuich et al., 2014). The raw data were first normalized to cinnamic acid tracer (Table S5A) and then aggregated by calculating concentration means [pmol] for each metabolic compound over the experimental replicates performed per biologically independent experiment, with one experiment for biological replicate 1, three experiments for biological replicate 2 and two experiments for biological replicate 3 (Table S5B). For compounds for which multiple derivatization products (Main product MP and Byproduct BP) were present at all time points, MP and BP were combined and listed as 'Sum'. In these cases the MP + BP sums were used for further analyses. If a derivatization product was not identified at all time points, the MP - present in most or all time points - was used for further analyses. As not all metabolites could be detected in uninfected cultures, mean metabolite concentrations were normalized to the means of the 12 h time point data from both non-infected and infected measurements of all replicates (Table S5C), followed by log2 transformation. For single time-point analysis, log2 values of the fold-changes from Table S5C (represented in Table S5D) were calculated for visualization. Statistical analysis was done for the 48 h infection time-point for each metabolite (mean, P values, difference of means and standard error (SE) of difference). The significance was calculated via multiple, unpaired t-tests (Table S5E). Significantly altered metabolites ($P < 0.05$) for the 48 h time point are displayed in an interactive pathway map in Figure 3. In order to correct for continued cell growth during the time-course experiments, data in Table S5C were used for calculating ratios of infected versus non-infected states for each time point (Table S5F). The log2 values of the ratios of the fold changes between infected and non-infected (Table S5G) are presented as time-course diagrams in Figure S2.

Analysis of *In Vivo* Experiments

Sample sizes were determined with the software PS: Power and Sample Size Calculations (http://biostat.mc.vanderbilt.edu/wiki/Main/PowerSampleSize). Calculations were done for two-tailed t-tests for treated and control groups (ratio 1:1) to reject the null hypothesis with a power of 0.8 (probability of Type 1 error = 0.05 and of Type 2 error 1-0.8 = 0.20). The parameters taken into account for this calculation were the expected bacterial load and cytokine levels in lung homogenate. The minimal difference to be achieved between the means of buffer- and substance-treated mice was thereby 25% of that found in preliminary experiments using tetracycline as positive control. For statistical comparison of the two groups of *Ctr*-infected mice receiving either MMF or buffer 2-way

ANOVA with Bonferroni post-test (body weight) or Mann–Whitney test (histological score and log-transformed bacterial load, cytokines and MPO) were conducted using the software GraphPad Prism.

DATA AND SOFTWARE AVAILABILITY

Primary hits of the human genome-wide RNAi screen for host cell factors essential for *Chlamydia* infection are reported in Table S1; validated hits from secondary screening in Table S2. Metabolite data acquired by GC-MS are listed in Table S5.

Cell Host & Microbe, Volume *23*

Supplemental Information

Combined Human Genome-wide RNAi and Metabolite Analyses Identify IMPDH as a Host-Directed Target against *Chlamydia* Infection

Marion Rother, Erik Gonzalez, Ana Rita Teixeira da Costa, Lea Wask, Isabella Gravenstein, Matteo Pardo, Matthias Pietzke, Rajendra Kumar Gurumurthy, Jörg Angermann, Robert Laudeley, Silke Glage, Michael Meyer, Cindrilla Chumduri, Stefan Kempa, Klaus Dinkel, Anke Unger, Bert Klebl, Andreas Klos, and Thomas F. Meyer

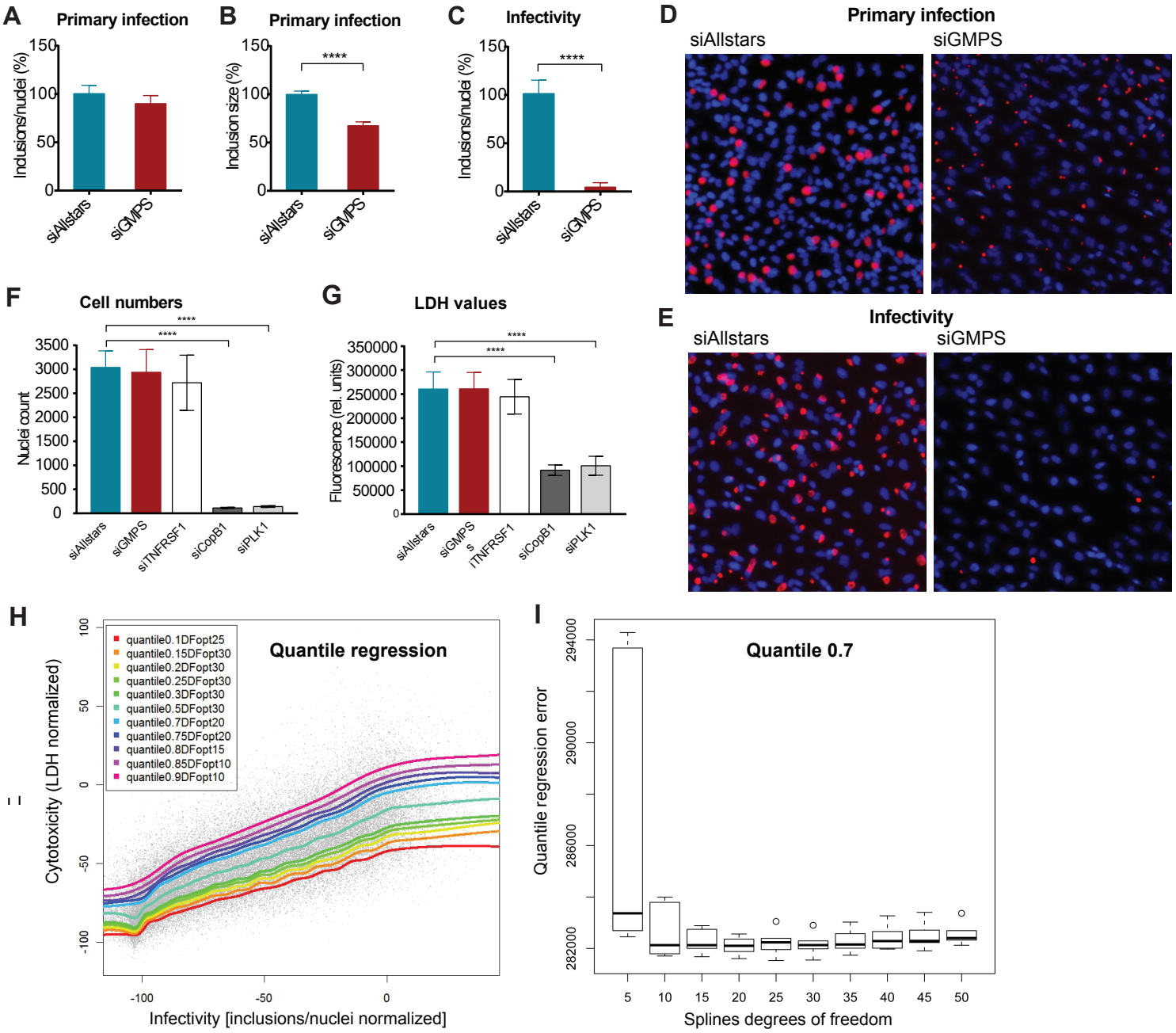

Figure S1 Related to Figure 1.
(A-C) Establishment and performance of screening controls. Cells were seeded in 384 wells and reversely transfected with neutral (siAllstars) and inhibiting siRNA control (siGMPS). After 3 d, cells were infected with CTL2 at MOI 0.3. Primary infection cells were fixed 24 h p.i. For quantification of infectious progeny cells were lysed 48 h p.i., lysate was titered onto fresh cells, which were fixed 24 h later. Inhibiting control siGMPS led to smaller inclusion size in primary infection and strong reduction in formation of infectious progeny, while inclusion number was not significantly altered in primary infection. Knockdown thus disturbs intracellular growth but not invasion of CTL2. Data show mean ± SD of three independent experiments;**** $P < 0.0001$, two-tailed Mann-Whitney test. (D) Corresponding representative IF images of siAllstars- and siGMPS-transfected cell 24 h after infection (primary infection) and (E) resulting infectivity. Nuclei, blue. CTL2 inclusions, red. Upon knockdown with the inhibitory screening control siGMPS inclusions in primary infection are smaller compared to neutral control siAllstars and resulting infectivity is strongly reduced. (F) Quantification of transfected cells. Cells were seeded in 384 wells and reversely transfected with siAllstars, siGMPS and cytotoxic (siCopB1 and siPLK1) siRNA controls, as described above. Nuclei count in primary infection was determined using automated microscopy and resulting LDH activity from lysates prepared 48 h p.i. was assessed in parallel (G), demonstrating high correlation between original cell count and resulting total LDH activity. Data show mean percentage of LDH activity ± SD of three independent experiments; ***$P < 0.0001$, one-way ANOVA with Bonferroni post-hoc test. (H) The optimal splines are displayed for the quantiles 0.1, 0.15, 0.2, 0.25, 0.3, 0.5, 0.7, 0.75, 0.8, 0.85, 0.9 and the optimal DF for each reported in the legend. For every quantile value, the “extreme” genes were determined, i.e. the genes whose LDH values lie below the quantile curves for quantiles 0.1, 0.15, 0.2, 0.25, 0.3 and above those for 0.7, 0.75, 0.8, 0.85, 0.9. (I) Boxplots derived from the five test errors for quantile 0.7. Quantile regression errors calculated for quantile 0.7 are displayed for degrees of freedom from 5 to 50 with intermitting steps of 5. The minimal median error is obtained for DF=20 and is very small. The number of training data is high with respect to the DF, so overfitting is small for all tested DFs. For DF=5 underfitting can be observed, i.e. the approximating function is too rigid to account for the variation in the data. See also Table S1. Abbreviations: siGMPS – siRNA targeting guanosine monophosphate synthase; siTNFRSF1 – siRNA targeting tumor necrosis factor receptor superfamily, member 1A; siCopB1 – siRNA targeting coatomer protein complex subunit beta 1; siPLK1 – siRNA targeting polo-like kinase 1.

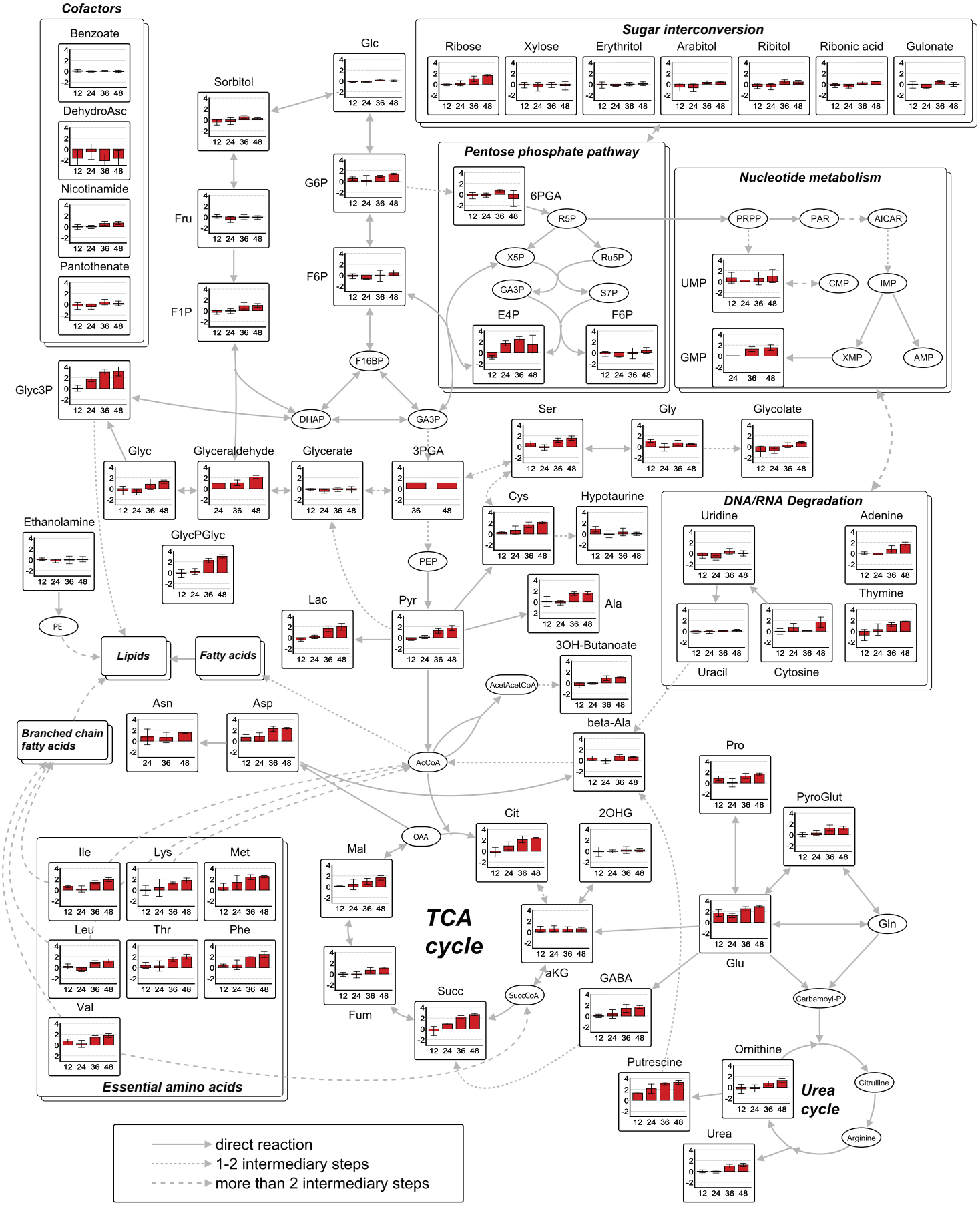

Figure S2 Time course data of metabolite regulation in *Chlamydia*-infected cells. Related to Figure 2.
HeLa cells were infected with CTL2 at MOI 1 or left uninfected for 12, 24, 36 and 48 h in three biological replicates. Diagrams represent the log2 values of the ratios of the fold changes between infected and non-infected samples (mean ± SD). For single time-point data see Table S5. A detailed description of data processing and normalization is provided in the methods section. Abbreviations of metabolites: 2OHG: 2-Hydroxyglutarate; 3OH-Butanoate: (D)-3-Hydroxybutyrate; 3PGA: 3-Phosphoglyceric acid; AcCoA: Acetyl Coenzyme A; AcetAcetCoA: Acetoacetyl-CoA; aKg: alpha-Ketoglutaric acid; Ala: Alanine; Asn: Asparagine; Asp: Aspartate; Beta-Ala: beta-Alanine; Carbamoyl-P: Carbamoyl-phosphate; Cit: Citrate; Cys: Cysteine; DehydroAsc: dehydroascorbic acid; DHAP: Dihydroxyacetone phosphate; E4P: Erythrose 4-phosphate; F16BP: Fructose-1-6-bisphosphate; F1P: Fructose-1-phosphate; F6P: Fructose-6-phosphate; Fru: Fructose; Fum: Fumarate; G6P: Glucose-6-phosphate; GA3P: Glyceraldehyde 3-phosphate; GA3P: Glyceraldehyde 3-phosphate; GABA: gamma-Aminobutyric acid; Glc: Glucose; Gln: Glutamine; Glu: Glutamate; Gly: Glycine; Glyc: Glycerol; Glyc3P: Glycerol-3-phosphate; GlycPGlyc: Glycerophosphoglycerol; Ile: Isoleucine; Lac: Lactate; Leu: Leucine; Lys: Lysine; Mal: Malate; MP:Main product detected by GC-MS; Met: Methionine; OAA: Oxaloacetic acid; PE: Phosphatidylethanolamine; PEP: Phosphoenolpyruvate; PG6: Phosphogluconolactone; Phe: Phenyl-alanine; Pro: Proline; Pyr: Pyruvate; PyroGlut: Pyro-glutamate; R5P: Ribose-5-phosphate; Ru5P: Ribulose-5-phosphate; S7P: D-Sedo Heptulose 7-P; Ser: Serine; Succ: Succinate; SuccCoA: Succinyl Coenzyme A; Thr: Threonine; Val: Valine; X5P: Xylulose 5-phosphate. See also Table S5.

A

MPA parameter	2 mg/kg IV	40 mg/kg PO
t1/2 (h)	4.57	6.99
Tmax (h)		0.08
Cmax [ng/mL]		7982.30
C0 [ng/mL]	15176.20	
AUC 0-inf [h*ng/mL]	8765.60	17486.70
Vss [l/kg]	0.72	
Cl [l/h/kg]	0.17	
F (%)		9.40

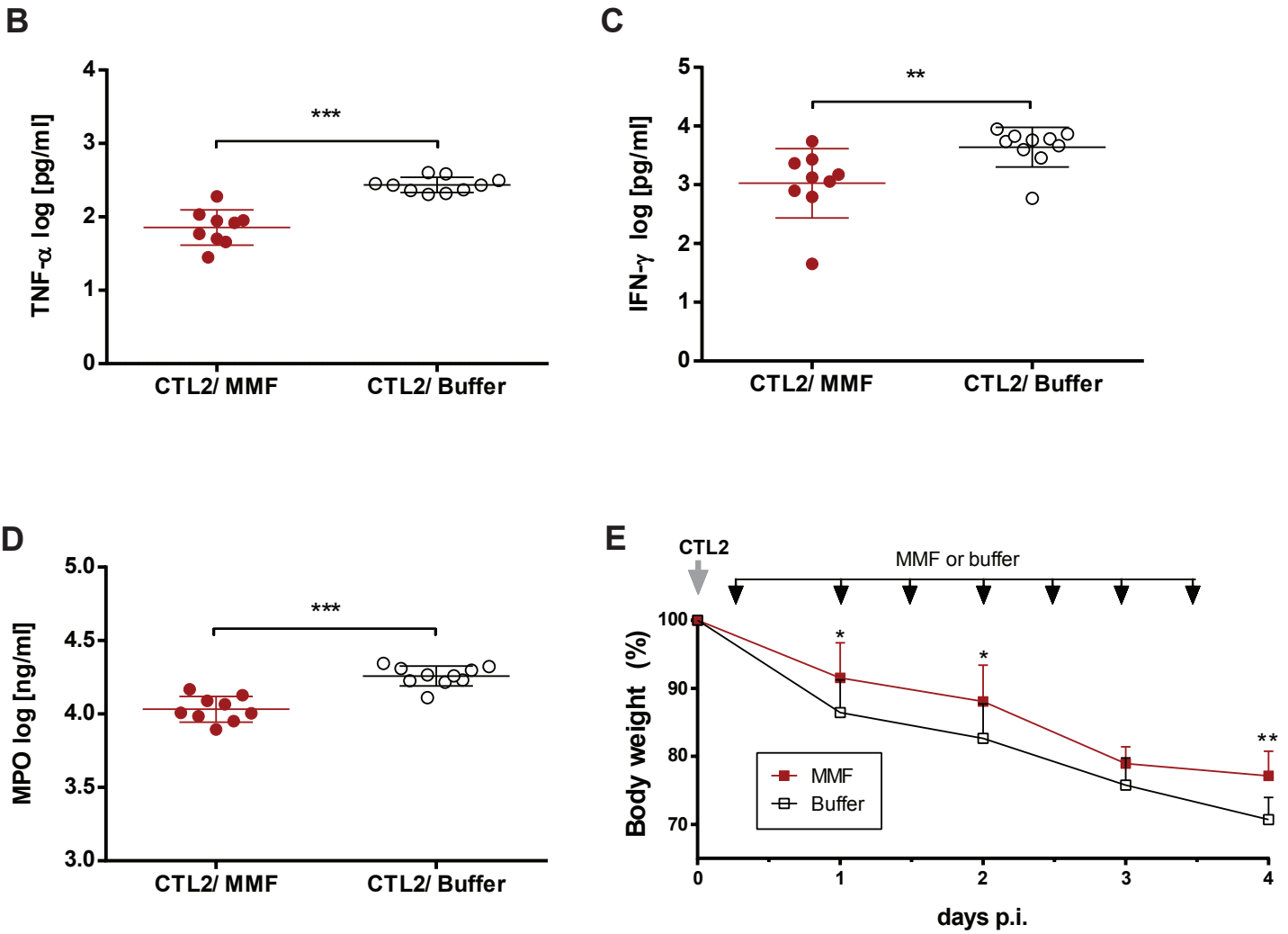

Figure S3 Related to Figure 4.
Pharmacokinetic parameters of the active metabolite mycophenolic acid (MPA) after administration of single doses of 2 mg/kg mycophenolate mofetil (MMF) IV and 40 mg/kg MMF PO to male C57BL/6J mice (**A**). t1/2 [h] - half-life; Tmax [h] - time at which Cmax is observed; Cmax [ng/ml] - maximum plasma drug concentration; C0 [ng/ml] - estimated initial (zero-time) plasma drug concentration; AUC 0-inf [h*ng/ml] - area under the plasma drug concentration-time curve (from zero to infinity); Vss [l/kg] - steady-state volume of distribution; CL [l/h/kg] – clearance; F [%] – bioavailability.
Ten to 12-week old male C57BL/6J mice were intranasally infected with a CTL2 IFU of 8 × 105; 200 mg/kg of MMF was orally applied bidaily starting 6 h p.i., whereas infected control mice received buffer only (arrows in panel E). All mice were sacrificed on day 4 p.i., and in homogenates from right lung lobes levels of TNF-α (**B**) and INF-γ (**C**) and the granulocyte marker enzyme myeloperoxidase (MPO) (**D**) were determined. Mice were monitored daily and body weight was documented (**E**). Mean and standard deviation of n = 10 mice in each group are depicted, *P < 0.05; **P < 0.01; ***P < 0.001.